# X-ray Properties of Young Stellar Objects in OMC-2 and OMC-3 from the *Chandra* X-ray Observatory

Masahiro Tsujimoto and Katsuji Koyama
*Department of Physics, Graduate School of Science, Kyoto University, Sakyo-ku, Kyoto, 606-8502, Japan*
tsujimot@cr.scphys.kyoto-u.ac.jp, koyama@cr.scphys.kyoto-u.ac.jp

Yohko Tsuboi
*Department of Physics & Astrophysics, 525 Davey Laboratory, Pennsylvania State University, University Park, PA 16802, USA*
tsuboi@astro.psu.edu
and

Miwa Goto and Naoto Kobayashi
*National Astronomical Observatory of Japan, 650 North A'ohoku Place, Hilo, HI 96720, USA*
mgoto@subaru.naoj.org, naoto@subaru.naoj.org

## ABSTRACT

We report X-ray results of the *Chandra* observation of Orion Molecular Cloud 2 and 3. A deep exposure of $\sim 100$ ksec detects $\sim 400$ X-ray sources in the field of view of the ACIS array, providing one of the largest X-ray catalogs in a star forming region. Coherent studies of the source detection, time variability, and energy spectra are performed. We classify the X-ray sources into class I, class II, and class III + MS based on the $J$, $H$, and $K$-band colors of their near infrared counterparts and discuss the X-ray properties (temperature, absorption, and time variability) along these evolutionary phases.

*Subject headings:* stars: pre-main sequence — X-rays: stars — infrared: stars — Individual: OMC-2, OMC-3

## 1. INTRODUCTION

Stars are known to possess high energy phenomena well before they reach the main sequence (MS)[1]. The *Einstein* observatory discovered that PMS stars (class III and class II stage with ages of $\sim 10^7$ and $\sim 10^6$ years after the on-set of gravitational collapse, respectively) are strong X-ray emitters (Feigelson & DeCampli 1981; Montmerle et al. 1983). Successive observations with *ASCA* and *ROSAT* detected hundreds of X-ray samples of PMS stars with better spectral or spatial resolution. They revealed that the X-ray activities in these objects are quite common. Koyama et al. (1996) and Kamata et al. (1997) moved the start of X-ray activity forward to protostars. They detected hard X-rays from class I ($\sim 10^5$ years) protostars with *ASCA*. Recently, Tsuboi et al. (2001) reported hard X-ray emission from two class 0 candidates in the Orion Molecular Cloud (OMC) using the *Chandra* X-ray Observatory (CXO). Now

[1]In this paper, we define terminologies as follows; "Protostars" are class 0 and class I objects. "Pre-main sequence (PMS) stars" and "T Tauri Stars (TTS)" are class II and class III objects. TTS comprise two subclasses, Classical T Tauri Stars (CTTS) and Weak-line T Tauri Stars (WTTS), corresponding to class II and class III, respectively. "Young Stellar Objects (YSO)" are class 0, I, II, and III sources collectively.

YSOs at virtually all the evolutionary phases — from class 0 to class III — are known to emit X-rays.

However, the X-ray emission mechanism has not been well understood. Imanishi, Koyama, & Tsuboi (2001) observed the $\rho$-Ophiuchi dark cloud with the CXO and found that the X-ray emitting regions of several sources are well beyond their stellar surface. This may be explained if the X-rays are due to star-disk magnetic interaction. Grosso et al. (2000) reported, on the other hand, that the X-ray emission does not depend on the existence of disks; no significant difference of the X-ray luminosity function is seen between *ROSAT*-detected class III objects (no disk) and class II objects (with disks). Montmerle et al. (2000) advocated that the reconnection of magnetic loops between stellar surface and disk is responsible for quasi-periodic flares and extremely high luminosity X-rays found in a protostar (YLW16) with *ASCA* (Tsuboi et al. 2000). Schulz et al. (2001) detected high temperature plasma with moderate luminosity and no rapid variability from YSOs in the Orion Nebula Cluster with the CXO. Hence they argued that the stellar surface-disk arcade model is unlikely but magnetically confined stellar plasma is a more likely origin for the X-ray activities, as was suggested by Skinner & Walter (1998) based on the *ASCA* observation of a CTTS (SU Aur). These arguments from previous studies may not be disagreements with each other, but are far from a unified picture of X-ray emission from YSOs.

Orion Molecular Cloud 2 and 3 (OMC-2 and OMC-3), located at a distance of $\sim$ 450 pc from us, are the best sites to study X-ray properties of YSOs at various evolutionary phases from class 0 through class III. X-rays from class 0 candidates have only been reported in OMC-3 (Tsuboi et al. 2001). Therefore, this cloud is the unique site where we actually provide X-ray samples from class 0 to class III. Moreover, the moderate angular size allows us to fully cover the clouds in the CXO/ACIS field of view (FOV).

Here, we report results of the CXO observation of the OMC-2 and OMC-3 star forming regions, with one of the deepest exposures of star forming regions. The purposes of this paper are 1) to conduct a coherent study of the X-ray source detection, time variability, and energy spectra, and to provide a catalog of one of the largest samples of X-ray sources in a star forming region, and 2) to investigate the X-ray properties of YSOs as a function of evolutionary phase inferred from the near infrared (NIR) data, and to compare them with the results of other star forming regions.

For the second purpose we use the 2MASS data, which is the deepest currently available in these regions. We conducted deeper infrared surveys on these clouds down to $\sim$ 18 mag in the $J$, $H$, and $K$-band. Those results will be presented in a separate paper.

## 2. OBSERVATION

The observation of OMC-2 and OMC-3 was carried out on 2000 January 1–2 using the CXO with a nominal exposure time of 89.2 ksec. We used four ACIS-I chips (I0, I1, I2, and I3) and one ACIS-S chip (S2) on the focal plane of the mirror system. All these detector chips utilize front-illuminated CCDs, which have sensitivity over a wide energy range (0.2–10.0 keV) with moderate energy resolution ($\Delta E \sim 200$ eV at $E = 6$ keV). Together with the optics, ACIS achieves sub-arcsec spatial resolution for on-axis sources, and a $8\farcm4 \times 8\farcm4$ FOV for each CCD chip. Details on the satellite and the detectors are found in Weisskopf, O'dell, & van Speybroeck (1996) and Garmire et al. (2001), respectively.

Its spectroscopic capability in the hard energy band, together with the sub-arcsec spatial resolution, makes the CXO/ACIS an ideal instrument for the observation of star forming regions, where sources are heavily absorbed and crowded.

Figure 1 shows the FOV of our observation overlaid on the 1300mm intensity contour map (Chini et al. 1997). OMC-2 and OMC-3 are separated into south and north by the dotted line. Our observation fully covers both star forming clouds.

## 3. DATA REDUCTION AND ANALYSIS

### 3.1. Data Reduction

For the data reduction, we use the level 2 data "reprocessed" at the Chandra X-ray Center (CXC). This version improves the aspect solution and restores the degradation of energy gain and resolution due to the increase of the charge trans-

fer inefficiency (CTI) of the ACIS[2]. For data manipulation, we use the Chandra Interactive Analysis of Observations (`CIAO`) version 2.1 and `FTOOLS` version 4.2.

In order to avoid the "spiking" problem reported by the CXC[3], we manually randomize the values of `ENERGY` and `PI` columns in the event file. After this procedure, we conduct the analysis in the following sections separately for the ACIS-I and ACIS-S data. Throughout this paper, we use X-ray photons in the 0.5–8.0 keV energy band. The photons of each source are accumulated from an elliptical region. The major and minor axes, and the rotation angles are derived from the `wavdetect` command.

### 3.2. Source Finding

We use `wavdetect` command with the significance criterion of $1 \times 10^{-5}$ and the wavelet scales ranging from 1 to 16 pixels in multiples of $\sqrt{2}$. We remove a few spurious sources through careful inspection by eye. We then detect 365 sources in the 0.5–8.0 keV band image. In order to pick up either soft (less absorbed) or hard (highly absorbed) sources more effectively, we also apply the same detection algorithm to the 0.5–2.0 keV (soft) and 2.0–8.0 keV (hard) band image. Then 17 and 16 new sources are found in the hard band and the soft band image, respectively. In total, we detect 398 X-ray sources in the ACIS-I and ACIS-S FOV. For each detected source, we calculate the X-ray photon count (0.5–8.0 keV) and the hardness ratio (Table 1).

For a systematic study, we divide all the X-ray sources into two groups, "bright" ($> 200$ counts) and "faint" ($\leq 200$ counts) sources, according to the photon counts inside the accumulation region. Out of 398 sources, 136 sources are "bright", and 262 are "faint". If the X-ray counts of the "bright" sources are less than 3 times the background counts in the photon accumulation region, we remove these sources and define the remaining 123 sources to be "bright2". This screening is practically necessary to comprise a good sample for spectral and timing analyses. In particular, those at large off-axis angles have the background counts comparable to 200 due to a rather large accumulation area, hence the background has a large impact on the quality of the source spectrum and light curve.

### 3.3. Correlation with 2MASS Sources

For all the detected X-ray sources, we search for a NIR counterpart using the Point Source Catalog in the 2MASS Second Incremental Data Release[4]. It covers the whole ACIS-I and ACIS-S FOVs, and provides us with the NIR source positions and their photometric data in the $J$, $H$, and $K_s$-band down to 15.8, 15.1, and 14.3 mag, respectively.

In the ACIS-I and ACIS-S FOVs, we find 638 2MASS sources. First, we search for the 2MASS sources nearest to each CXO source within $3''$ radius. Second, we conversely search for the CXO source nearest to each 2MASS source within $3''$ radius. Thus we pick up the nearest CXO-2MASS pairs. The systematic position off-sets of the CXO sources from their 2MASS counterparts is found to be $-0\farcs186$ and $0\farcs200$ in the direction of right ascension and declination. After correcting these systematic off-sets of the X-ray position, we reapply the same procedure for the 2MASS counterpart search. Finally we find that 238 out of 398 ($\sim 60\%$) X-ray sources have a 2MASS counterpart. The distance between X-ray sources and their counterparts is found to be $\sim 0\farcs5$.

Together with the X-ray properties, the $J$–$H$ and $H$–$K$ colors of their 2MASS counterparts are given in Table 1. About 80% of the "bright" sources have a 2MASS counterpart (111 out of 136), while for the "faint" sources, the ratio is about 50% (127 out of 262).

### 3.4. Timing Analysis

We make the X-ray light curve (background is not subtracted) for the "bright2" sources and perform $\chi^2$ fit with a constant flux assumption. We discriminate the time-variable sources by the significance criteria of 0.01, which are marked with † in Table 2. About 40% (47 out of 123) of the sample sources are found to be time-variable. Most of them show flare-like variability, a fast rise and slow decay of the flux. Some light curves show multiple flares during the observation. A variety

[2]see http://asc.harvard.edu/udocs/reprocessing.html

[3]see http://asc.harvard.edu/ciao/caveats/acis_pi.html

[4]see http://www.ipac.caltech.edu/2mass/

of features are seen in the light curves, and it is difficult to separate X-ray photons during the flare and at quiescence in a coherent manner. We therefore deal with them in the same way.

### 3.5. Spectral Analysis

We next perform spectral analysis of the "bright2" sources, the same data set for the timing analysis. We combine each energy bin so as to have more than 20 photons, then subtract a background spectrum. We use the `sherpa` program for the spectral fitting.

First we fit the spectrum of all the sample sources with a thin thermal plasma and a power-law model, both with absorption of hydrogen column density ($N_{\rm H}$). The free parameters of the former model are temperature ($k_BT$), metallicity ($Z$), and normalization, while the latter's are photon index ($\Gamma$) and normalization. The former model is accepted for 90 out of 123 sources with the upper probability of larger than 0.01 (99% confidence). The latter model is accepted for 64 sources, of which all except two are also accepted in the former model. On the contrary, both the models are rejected for the other 31 sources. Therefore, here and after, we use the results of the thin-thermal plasma model fittings (Table 2).

Second, for the 31 sources which reject both models, we try 2-component models, 1) a thin-thermal plasma + power-law and 2) 2-temperature thin-thermal plasma model. Additional free parameters are $k_BT$ (or $\Gamma$) and normalization. Both models are acceptable for 8 and rejected for 6 sources out of 31 samples, while the latter model are accepted by other 15 sources. We therefore use the results of the two temperature thin-thermal plasma model fittings (Table 3).

## 4. DISCUSSION

### 4.1. The Nature of X-ray and NIR Sources

#### *4.1.1. The Nature of NIR Sources*

Since some fraction of the 2MASS sources may be background or foreground sources, we first estimate the contribution of background galaxies in the following way. The number counts of galaxies per square degree per magnitude at a certain $K$-band (2.2$\mu$m) magnitude is given by

$$\frac{dN}{dK} = 4000 \times 10^{\alpha(K-17)} \quad (1)$$

where $\alpha = 0.67$ for 10 mag$< K <$ 17 mag (Tokunaga 2000). Therefore, the number in the range of $K_{min}$ mag$< K < K_{max}$ mag is

$$\int_{K_{min}}^{K_{max}} \frac{dN}{dK}\, dK = \frac{4000}{\alpha \log 10}\{10^{\alpha(K_{max}-17)} - 10^{\alpha(K_{min}-17)}\}. \quad (2)$$

The NIR counterparts of the CXO sources have a $K$-band flux of 6 mag $< K_s <$ 15 mag. We substitute $K_{min} = 6$ and $K_{max} = 15$ for simplicity, though equation (2) is valid only for $K_{min}$ >10 mag. Still, this gives us a good estimate, because the second term of the right hand side of equation (2) is negligible compared to the first term in this case. Considering our FOV ($8\farcm4 \times 8\farcm4$ for each chip), the estimated number of galaxies with 6 mag$< K_s <$ 15 mag is $\sim$12. This is only 1.9% of the 2MASS source number in our FOV. In addition, the background galaxies in this direction may suffer significant extinction due to molecular clouds, hence the contribution of extragalactic sources to our 2MASS sources should be even smaller than that estimated above.

We can also neglect the contribution of foreground sources to our 2MASS sample, because OMC-2 and OMC-3 lie off the galactic plane by $\sim$ 20 degrees. Thus, we can safely assume most of the NIR sources to be cloud members (YSOs and MS stars).

#### *4.1.2. The Nature of X-ray Sources*

Krishnamurthi et al. (2001) observed the core of the Pleiades star cluster with the CXO for 36 ksec, and found that a significant fraction of X-ray sources are likely to be AGNs. We therefore try to discriminate cloud members from extragalactic sources using the X-ray hardness ratio.

In Figure 2, the histogram of the hardness ratio is given separately for X-ray sources with and without a NIR counterpart. The hardness ratio of the X-ray sources with a NIR counterpart has the peak at $-1.0 \sim -0.8$, while those without a NIR counterpart has its peak at $0.2 \sim 0.4$. A power-law spectrum of $\Gamma$ =1.7 has the hardness ratio of $0.1 \sim 0.4$ when absorbed with the column density of $N_{\rm H}$=1–2$\times10^{22}$cm$^{-2}$, a typical value of

the cloud column density. This corresponds to the peak of X-ray sources without a NIR counterpart. On the contrary, a thin-thermal spectrum with $k_BT$= 1.2 keV, $Z$=0.20, and $N_{\rm H}$= $10^{21}{\rm cm}^{-2}$, typical values for class III and MS stars (see the following section), has the hardness ratio of $\sim -0.8$. This corresponds to the peak of the histogram of X-ray sources with a NIR counterpart.

Therefore, X-ray sources with a NIR counterpart are mostly cloud members, consistent with the conclusion of the previous subsection. We thus focus on the X-ray sources with a NIR counterpart. X-ray sources without a NIR counterpart, on the other hand, are probably AGNs, which are not the main subject of this paper.

### 4.2. Classification

YSOs are observationally classified into class 0 through class III based on their spectral energy distribution (SED) from optical, NIR, mid infrared (MIR), and sub-mm bands (André & Montmerle 1994). Since no systematic catalog for wavelengths longer than MIR is published in both of these clouds, we use the $J$–$H$/$H$–$K$ color-color diagram of the 2MASS counterparts for the classification (Lada & Adams 1992; Strom, Kepner, & Strom 1995).

Out of the 123 "bright2" sources, 108 are detected either in the $J$, $H$, or $K_s$-band, and the remaining 15 are found in none of these bands. Figure 3 shows the $J$–$H$ vs $H$–$K$ plots of the detected X-ray sources.

Intrinsic colors for giants and dwarfs are taken from Tokunaga (2000) with colors transformed into the CIT system (Bessel & Brett 1988), while CTTS locus is taken from Meyer, Calvet, & Hillenbrand (1997). We assume the slope of the reddening lines to be $E(J\text{–}H)/E(H\text{–}K) = 1.63$ (Martin & Whittet 1990). All the 2MASS colors are also translated into CIT color system with the transformation formula established by Carpenter (2001).

Based on the position in this diagram, we classify the sources into three groups — class I, class II, and class III + MS — in the following way[5]. Class I and class II sources are characterized by $H$–$K$ color excess over $J$–$H$ color, originating from their disk emission, while class III and MS sources are not. Therefore, sources between the second and the third leftmost reddening lines, and above the CTTS locus are either class I or class II sources. Class I and class II sources in this region can be distinguished from each other by the amount of extinction, where class Is generally have higher extinction (typically $J$–$H$>1.5) than class IIs (Lada & Adams 1992; Strom, Kepner, & Strom 1995). Therefore, sources with $J$–$H$>1.5 are classified to be class I and $J$–$H\leq$ 1.5 are class II. Sources between the leftmost and the second leftmost reddening lines can be either class I, class II, class III or MS stars. In this region again, we classify sources based on their amount of extinction; sources with $J$–$H$>1.5 are class I, $J$–$H$>0.8 are class II, and $J$–$H\leq$0.8 are class III + MS. These criteria are based on the fact that, in the Taurus-Auriga dark cloud complex, class II sources rarely have larger extinction than $J$–$H$>1.5 and class III sources rarely have larger extinction than $J$–$H$>0.8 (Strom, Kepner, & Strom 1995). In addition, sources which lack 2MASS $J$ and/or $H$-band detection (the upper limit of the $H$-band magnitude is given) are classified as class I, because all of them have larger extinction of $H$–$K$>1.2 mag.

Then, out of the 108 sources, we find 19 class I, 18 class II, and 61 class III + MS sources. The other 10 are outside of the classification regions. The results are summarized in Table 2.

### 4.3. X-ray Properties of Different Classes

Based on the classification described in the previous section, we list the X-ray properties (absorption, metallicity, luminosity, and temperature) of each class in Table 4 and compare them with each other.

[5]Note that our classification based only on three NIR bands may be less complete compared with the conventional classification scheme. The number of class I and class II sources might be underestimated because the J-H/H-K diagram is not very sensitive to the NIR excess (Olofsson et al. 1999; Persi et al. 2000; Bontemps et al. 2001). On the other hand, the number of class I and class II sources might be overestimated because we can not discriminate mildly extinguished class III + MS from them. Therefore it may be fair to use the terminology "class I-like" instead of "class I" etc. For simplicity, however, we use the latter terminology in this paper.

#### 4.3.1. Absorption

The X-ray absorption decreases as a YSO evolves from class I through class III + MS. This is basically consistent with the fact that we classify these sources using their NIR extinction. $J$–$H$ derived from the NIR photometry is a good indicator for the amount of material in solid-state, while $N_{\rm H}$ derived from X-ray spectroscopy represents the amount of gas. Therefore, $N_{\rm H}$ should go in proportion to $J$–$H$, and the ratio gives us the information of the dust-to-gas ratio in a star forming cloud.

For all the "bright2" sources with NIR data, we plot the relation between $N_{\rm H}$ and $J$–$H$ (Figure 4). A clear correlation is found. The best-fit linear function is

$$N_{\rm H}/10^{22}\,{\rm cm}^{-2} = (1.35\pm0.18)\{(J\text{–}H)-(0.63\pm0.05)\}\ {\rm mag}. \quad (3)$$

The $J$–$H$ offset of 0.63±0.05 mag should be the averaged intrinsic color after removing the reddening, which corresponds to the spectral type K5–K7 in MS stars (Tokunaga 2000). This indicates that low mass YSOs and MS stars are dominant in these clouds. The slope of 1.35±0.18 gives us information on the dust-to-gas ratio. Together with the relation between $A_V$ and $J$–$H$ given in Meyer et al. (1997),

$$N_{\rm H}/10^{21}\ {\rm cm}^{-2} = (1.49 \pm 0.20) \times {\rm A_V\ mag} \quad (4)$$

is derived. The slope of 1.49±0.20 is smaller than those of the Galactic interstellar medium and the $\rho$-Ophiuchi dark cloud, and is similar to that of another star forming region, the Mon R2 cloud (Predehl & Schmitt 1995; Imanishi et al. 2001; Kohno, Koyama, & Hamaguchi 2001). Thus the dust-to-gas ratio may scatter from cloud to cloud, possibly with more massive star forming regions having larger dust-to-gas ratio.

#### 4.3.2. Metallicity

We determine the metallicity for many sample stars in a star forming region for the first time. A hint of a decreasing trend toward evolved classes is seen, although this depends on the way the samples are broken into class I, class II, and class III + MS. The metallicity, when all classes are combined, is 0.45 (0.37–0.52) solar.

Padgett (1996) observed 30 G and K pre-main-sequence stars in the nearby star forming regions including Orion, and studied their photospheric abundances using the iron absorption lines in the optical band. All star forming regions are found to have the solar abundance.

The discrepancy between the coronal abundance and the photospheric abundance, which are derived from the X-ray observations and the optical observations respectively, is often seen in other samples Yamauchi et al. (1996); Imanishi et al. (2001).

#### 4.3.3. Luminosity and Temperature

The temperature ($k_BT$) and the luminosity ($L_X$) are plotted on Figure 5, separately for class I, class II, and class III + MS. The temperatures of class I to class III + MS sources are randomly distributed over a wide range of luminosity, but the mean temperatures of class I and class II sources are significantly higher ($k_BT \sim$ 3.0 keV) than that of class III + MS ($k_BT \sim$ 1.2 keV). We may argue that there are two types of X-ray emission mechanisms; one exhibits higher temperature, and the other has lower temperature. The former dominates in less evolved YSOs, like class I and class II sources, while the latter gradually appears as YSOs evolve to class III + MS. In this context, it is suggestive that most sources with two temperature components (Table 4) belong to class III + MS. The higher temperature component of these sources has $\sim$ 2.3 keV on average similar to the 1-temperature sources of class I and class II, while the mean of the lower temperature component is $\sim$ 0.8 keV similar to the 1-temperature sources of class III + MS. We hence suspect that the two component class III + MS sources may be in the transition phase between higher-temperature-dominant and the lower-temperature-dominant stage.

#### 4.3.4. Time Variation

Class II sources have a slightly higher fraction of time-variable sources than other classes, though it is not statistically significant. When class I and class II are combined and are compared with class III + MS, we see no significant difference in time-variation rate (in both groups, $\sim$ 40% are time-variable). Imanishi et al. (2001) also argues

that no significant difference of the flare rate is seen among three classes in the $\rho$-Ophiuchi dark cloud. Whether time-variable activity is related to the higher-temperature or the lower-temperature-component is not clear in our data set.

## 5. SUMMARY

We observed OMC-2 and OMC-3 with the CXO/ACIS for $\sim$ 100 ksec. This is one of the deepest observations ever performed in star forming regions in the X-ray band. We detected $\sim$ 400 X-ray sources in our FOV. Coherent analyses on these sources derived the following results.

1. Imaging analysis is performed for all the detected sources, and their position, photon counts, and hardness ratio are derived. This is one of the largest catalogs of X-ray sources in a star forming region.

2. Correlations with the 2MASS sources are found using the 2MASS database. About 60% of the X-ray sources have a NIR counterpart.

3. Spectral and timing analysis are performed for "bright2" X-ray sources. A one temperature thin-thermal plasma model can explain most of the spectra. About 40% of the "bright2" sources are found to be time-variable.

4. Most of the X-ray sources with a NIR counterpart are likely cloud members, while those with no NIR counterpart are probably background AGNs.

5. We classify the cloud members to be class I, class II, and class III + MS based on the $J$–$H$/$H$–$K$ color-color diagram and conduct a systematic comparison on the X-ray properties, such as absorption, luminosity, temperature, and time-variation.

6. Class I and class II sources are found to have higher temperatures than class III + MS. We thus propose that two types of X-ray emission mechanisms exist (higher temperature and lower temperature component). The higher temperature plasma appears in the earlier phase and lower temperature plasma appears as YSOs evolve. In the transition phase, possibly early class III, plasma emissions with different temperatures coexist.

7. The ratio of time-variable sources is nearly the same among different classes. Whether the time-variability is related to higher-temperature- or lower-temperature-plasma is still an open question.

The authors express their thanks to Dr. Yoshitomo Maeda for giving us invaluable information on the analysis of the ACIS data, especially on the source detection algorithm and detector calibrations. The authors also acknowledge the careful reading of the manuscript by Jun Yokogawa and Leisa Townsley. M.T. and M.G. are financially supported by the Japan Society for the Promotion of Science.

## REFERENCES


André, P. & Montmerle, T. 1994, ApJ, 420, 837

Bessel, M. S. & Brett, J. M. 1988, PASP, 100, 1134

Bontemps, S. et al. 2001, A&A, 372, 173

Carpenter, J. M. 2001, AJ, 121, 2851

Chini, R., Reipurth, B., Ward-Thompson, D., Bally, J., Nyman, L-Å, Sievers, A., & Billawala, Y. 1997, ApJ, 474, L135

Feigelson, E. D. & DeCampli 1981, ApJ, 243, L89

Garmire, G. P., et al., 2001, in preparation

Grosso, N., Montmerle, T., Bontempts, S., André, P., & Feigelson, E. D. A&A, 359, 113

Imanishi, K., Koyama, K., & Tsuboi, Y. 2001, ApJ, in press

Kamata, Y., Koyama, K., Tsuboi, Y., & Yamauchi, S. 1997, PASJ, 49, 461

Kohno, M., Koyama, K., & Hamaguchi, K. 2001, in preparation

Koyama, K., Hamaguchi, K., Ueno, S., & Kobayashi, N. 1996, PASJ, 48, L87

Krishnamurthi, A., Reynolds, C. S., Linsky, J.L., Martin, E., & Gagné, M. 2001, AJ, 11, 337

Lada, C. J. & Adams, F. C. 1992, ApJ, 393, 278

Martin, P. G. & Whittet, D. C. B. 1990, ApJ, 357, 113

Meyer, M. R., Calvet, N., & Hillenbrand, L. A. 1997, AJ, 114, 288

Montmerle, T., Koch-Miramond, L., Falgarone, E., & Grindlay, J, E. 1983, ApJ, 269, 182

Montmerle, T., Grosso, N., Tsuboi, Y., & Koyama, K. 2000, ApJ, 532, 1097

Morrison, R. & McCammon, D. 1983, ApJ, 270, 119

Oloffson, G. et al. 1999, A&A, 350, 883

Padgett, D. L. 1996, ApJ, 471, 847

Persi, P. et al. 2000, A&A, 357, 219

Predehl, P & Schmitt, J. H. M. M. 1995, A&A, 293, 889

Schulz, N. S., Canizares, C., Huenemoerder, D., Kastner, J. H., Tayler, S. C., & Bergstorm, E. J. ApJ, 549, 441

Skinner, S. L. & Walter, F. M. 1998, ApJ, 509, 761

Strom, K. M., Kepner, J., & Strom, S. E. 1995, ApJ, 438, 813

Tokunaga, A. T. 2000, in Allen's Astrophysical Quantities, ed. A. N. Cox, (4th ed.; New York: Springer-Verlag), 143

Tsuboi, Y., Imanishi, K., Koyama, K., Grosso, N., & Montmerle, T. 2000, ApJ, 532, 1089

Tsuboi, Y., Koyama, K., Hamaguchi, K., Tatematsu, K., Sekimoto, Y., Bally, J., & Reipurth, B. 2001, ApJ, 554, in press

Weisskopf, M. C., O'dell, S., & van Speybroeck, L. P. 1996, Proc. of SPIE, 2805, 2

Yamauchi, S., Koyama, K., Sakano, M., & Okada, K. 1996, PASJ, 48, 719



This 2-column preprint was prepared with the AAS LaTeX macros v5.0.

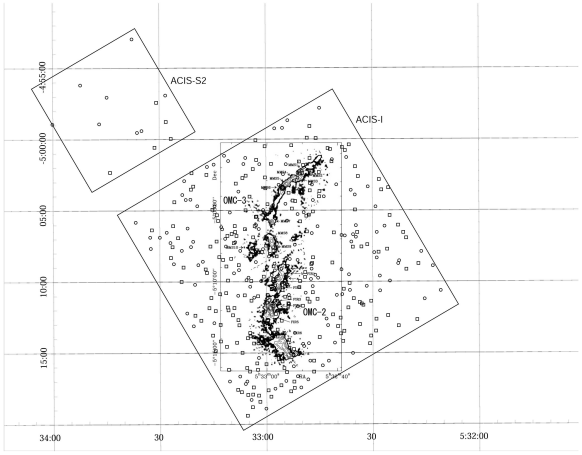


Fig. 1.— FOVs of ACIS-I (large square region) and ACIS-S2 (small square region at the top left) are overlaid on the 1300mm intensity map (Chini et al. 1997). ACIS-I covers the whole OMC-2 and OMC-3 star forming regions. Squares and circles are X-ray sources with and without a 2MASS counterpart, respectively. The coordinate is in the equinox 1950B.

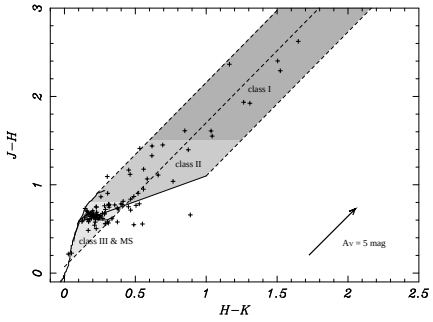


Fig. 3.— The $J$–$H$/$H$–$K$ color-color diagram in CIT color system. "Bright2" sources with the 2MASS $J$, $H$, and $K_s$-band detection are plotted (crosses). The typical error is $\pm 0.05$ mag. The evolution tracks of giants and dwarfs, and CTTS locus are given by solid lines, while the dotted lines represent the extinction vector. X-ray sources are classified into class I, class II, and class III + MS sources based on their position on the diagram.

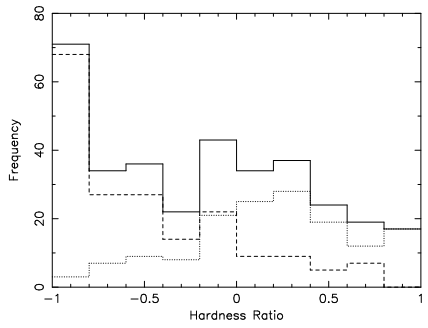


Fig. 2.— The histogram of the hardness ratio (from –1 to 1 with a step of 0.2) is shown by the dashed and dotted line for the X-ray sources with and without a NIR counterpart, respectively. The total is given by the solid line.

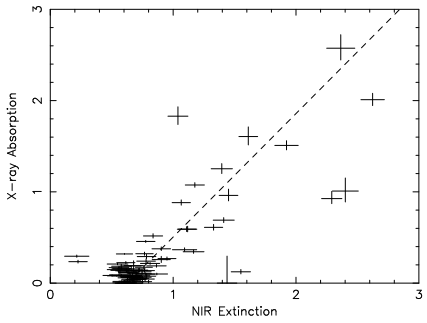


Fig. 4.— The NIR extinction ($J$–$H$ mag) and the X-ray absorption ($N_{\rm H}$ $10^{22}{\rm cm}^{-2}$) are plotted. The best-fit linear function is expressed with the dashed line.

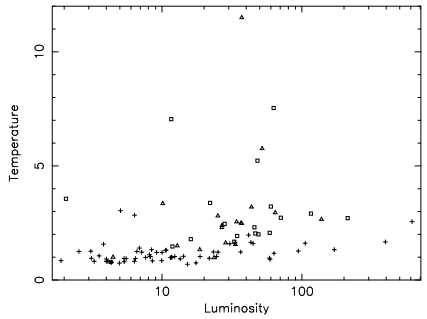


Fig. 5.— Luminosity ($10^{29}$ erg $s^{-1}$) in logarithmic scale and temperature (keV) of each source are plotted separately for class I (squares), class II (triangles), and class III + MS (crosses) sources.

Table 1

Results of Imaging Analysis and NIR Identification[a]

| ID[b] | Name[c] | X-ray[d] Counts | Hardness[e] Ratio | $J$–$H$[f] (mag) | $H$–$K$[f] (mag) |
|---|---|---|---|---|---|
| I1 | 053438.60-050844.6 | 255 | 0.31 | ··· | ··· |
| I2 | 053440.86-050700.0 | 63 | -0.02 | ··· | ··· |
| I3 | 053443.10-050919.8 | 368 | 0.62 | ··· | ··· |
| I4 | 053444.89-050650.9 | 403 | -0.54 | 0.725 | 0.379 |
| I5 | 053445.19-051046.9 | 176 | -0.25 | 0.748 | 0.517 |
| I6 | 053448.29-050714.9 | 535 | -0.66 | 0.658 | 0.223 |
| I7 | 053448.37-050502.9 | 549 | -0.77 | 0.675 | 0.188 |
| I8 | 053449.18-050440.0 | 127 | -0.97 | 0.695 | 0.227 |
| I9 | 053450.33-050639.9 | 70 | -0.29 | ··· | ··· |
| I10 | 053450.43-051113.0 | 773 | -0.75 | 0.663 | 0.172 |
| I11 | 053450.59-050651.6 | 110 | 0.40 | ··· | ··· |
| I12 | 053450.64-050409.4 | 361 | -0.70 | 0.720 | 0.289 |
| I13 | 053453.03-050328.7 | 1747 | -0.73 | 0.751 | 0.451 |
| I14 | 053453.42-051030.0 | 579 | -0.70 | 0.628 | 0.232 |
| I15 | 053453.45-050132.0 | 49 | 0.10 | 0.625 | 0.210 |
| I16 | 053453.71-050550.7 | 145 | -0.75 | 0.644 | 0.247 |
| I17 | 053455.38-050141.1 | 534 | -0.83 | 0.731 | 0.146 |
| I18 | 053455.66-050846.1 | 39 | 0.38 | ··· | ··· |
| I19 | 053455.76-050744.3 | 103 | 0.24 | ··· | ··· |
| I20 | 053456.07-050057.4 | 359 | -0.69 | 0.639 | 0.213 |
| I21 | 053456.13-050603.3 | 276 | -0.82 | 0.613 | 0.238 |
| I22 | 053456.64-050627.9 | 55 | 0.20 | ··· | ··· |
| I23 | 053456.67-050439.7 | 98 | 0.47 | ··· | ··· |
| I24 | 053456.71-051045.4 | 48 | -0.33 | 0.733 | 0.301 |
| I25 | 053456.82-051135.3 | 2286 | -0.82 | 0.713 | 0.467 |
| I26 | 053457.35-050605.8 | 19 | 0.58 | ··· | ··· |
| I27 | 053458.19-050929.7 | 558 | -0.71 | 0.762 | 0.283 |
| I28 | 053458.21-051156.4 | 258 | -0.64 | 0.604 | 0.219 |
| I29 | 053458.52-051228.8 | 135 | 0.04 | 0.552 | 0.236 |
| I30 | 053459.22-050128.0 | 28 | 0.43 | ··· | ··· |
| I31 | 053459.32-050531.8 | 740 | -0.75 | 0.767 | 0.313 |
| I32 | 053459.47-050827.4 | 30 | 0.27 | ··· | ··· |
| I33 | 053500.40-050946.6 | 213 | 0.13 | 0.567 | 0.310 |
| I34 | 053500.87-050941.2 | 135 | -0.72 | 0.559 | 0.318 |
| I35 | 053501.37-051107.9 | 60 | 0.33 | 0.962 | 0.575 |
| I36 | 053501.43-050934.6 | 670 | -0.85 | 0.668 | 0.180 |
| I37 | 053501.98-050045.0 | 63 | -0.46 | 0.631 | 0.219 |
| I38 | 053502.16-050440.3 | 83 | -0.76 | 0.757 | 0.374 |
| I39 | 053502.52-050411.8 | 11 | 0.82 | ··· | ··· |
| I40 | 053502.56-050500.3 | 9 | 1.00 | ··· | ··· |
| I41 | 053502.79-050305.7 | 20 | -0.40 | 0.576 | -0.065 |
| I42 | 053502.79-050003.7 | 1023 | -0.57 | 1.166 | 0.453 |
| I43 | 053502.85-050202.4 | 20 | 0.50 | ··· | ··· |
| I44 | 053503.12-050919.1 | 90 | -0.76 | 0.718 | 0.335 |
| I45 | 053503.30-050449.9 | 26 | 0.69 | ··· | ··· |
| I46 | 053503.33-051308.9 | 159 | 0.17 | ··· | ··· |
| I47 | 053503.41-050542.2 | 1771 | -0.62 | 0.216 | 0.027 |
| I48 | 053503.81-050520.9 | 17 | 0.53 | ··· | ··· |
| I49 | 053503.99-050142.9 | 20 | 0.70 | ··· | ··· |
| I50 | 053504.23-050844.3 | 54 | 0.26 | ··· | ··· |
| I51 | 053504.30-050814.7 | 25402 | -0.55 | 0.656 | 0.153 |
| I52 | 053504.45-050738.3 | 14 | -0.43 | ··· | ··· |
| I53 | 053504.55-045831.7 | 109 | -0.21 | 1.055 | 0.743 |
| I54 | 053504.64-050957.9 | 437 | -0.78 | 0.647 | 0.257 |
| I55 | 053505.24-045925.0 | 26 | 0.54 | ··· | ··· |
| I56 | 053505.65-045855.4 | 334 | -0.83 | 0.649 | 0.236 |
| I57 | 053505.66-050455.2 | 7 | 0.43 | ··· | ··· |
| I58 | 053505.76-051136.3 | 92 | -0.28 | 1.394 | 0.658 |
| I59 | 053505.95-050839.3 | 18 | -0.67 | 1.084 | 0.496 |
| I60 | 053506.09-051218.8 | 43 | -0.30 | -0.077 | -0.023 |
| I61 | 053506.36-050901.8 | 10 | 0.20 | ··· | ··· |
| I62 | 053506.49-045842.2 | 58 | -0.45 | 0.556 | 0.301 |
| I63 | 053506.58-050717.8 | 15 | 0.60 | ··· | ··· |
| I64 | 053506.61-050453.0 | 42 | 0.43 | ··· | ··· |

TABLE 1—*Continued*

| ID[b] | Name[c] | X-ray[d] Counts | Hardness[e] Ratio | $J$–$H$[f] (mag) | $H$–$K$[f] (mag) |
|---|---|---|---|---|---|
| I65 | 053506.71-051147.2 | 257 | -0.19 | 1.439 | 0.618 |
| I66 | 053506.83-051040.9 | 200 | -0.76 | 0.671 | 0.236 |
| I67 | 053507.54-051116.5 | 1232 | -0.21 | 1.066 | 0.584 |
| I68 | 053508.04-050120.0 | 14 | 0.14 | ··· | ··· |
| I69 | 053508.75-050442.3 | 26 | -0.85 | 0.742 | 0.356 |
| I70 | 053508.96-051027.4 | 12 | -0.67 | 0.615 | 0.095 |
| I71 | 053509.15-050648.9 | 1192 | -0.83 | 0.672 | 0.206 |
| I72 | 053509.32-045934.0 | 56 | 0.39 | ··· | ··· |
| I73 | 053509.42-045943.0 | 72 | -0.56 | 0.680 | 0.348 |
| I74 | 053509.85-045850.9 | 442 | 0.24 | ··· | 1.612 |
| I75 | 053510.14-051342.4 | 86 | 0.00 | ··· | ··· |
| I76 | 053510.32-051112.9 | 13 | 0.54 | ··· | ··· |
| I77 | 053510.51-045847.3 | 835 | 0.52 | ··· | 3.286 |
| I78 | 053511.56-050210.0 | 16 | 0.75 | ··· | ··· |
| I79 | 053511.81-051401.8 | 237 | -0.09 | ··· | ··· |
| I80 | 053512.72-051202.6 | 59 | -0.46 | 0.524 | 0.250 |
| I81 | 053512.80-050147.9 | 79 | -0.95 | 0.590 | 0.279 |
| I82 | 053512.92-045557.4 | 325 | 0.48 | ··· | ··· |
| I83 | 053512.95-050210.3 | 109 | -0.83 | 0.558 | 0.328 |
| I84 | 053513.00-050028.0 | 29 | 0.38 | ··· | ··· |
| I85 | 053513.34-050921.7 | 1088 | -0.74 | 0.683 | 0.189 |
| I86 | 053513.35-050416.3 | 7 | 0.71 | ··· | ··· |
| I87 | 053513.88-045805.0 | 207 | 0.11 | 2.364 | 1.164 |
| I88 | 053513.99-050740.6 | 21 | 0.81 | ··· | ··· |
| I89 | 053514.28-051428.1 | 268 | 0.01 | 2.401 | 1.504 |
| I90 | 053514.29-051342.1 | 116 | 0.00 | 1.941 | 1.264 |
| I91 | 053514.63-050627.1 | 34 | -0.65 | 1.156 | 0.653 |
| I92 | 053514.64-050226.5 | 312 | -0.82 | ··· | ··· |
| I93 | 053514.66-050314.2 | 574 | -0.85 | 0.676 | 0.183 |
| I94 | 053514.67-050854.1 | 33 | -0.76 | 0.572 | 0.282 |
| I95 | 053514.70-050828.0 | 4 | 1.00 | ··· | ··· |
| I96 | 053514.87-050650.6 | 333 | 0.16 | ··· | 1.216 |
| I97 | 053514.94-050120.1 | 24 | 0.58 | ··· | ··· |
| I98 | 053514.99-050715.0 | 62 | 0.71 | ··· | ··· |
| I99 | 053515.08-050655.4 | 112 | 0.21 | 2.294 | 1.198 |
| I100 | 053515.18-050758.2 | 4 | 0.50 | ··· | ··· |
| I101 | 053515.27-050034.4 | 29 | -0.86 | 0.631 | 0.256 |
| I102 | 053515.36-051342.0 | 68 | -0.53 | ··· | ··· |
| I103 | 053515.49-050114.0 | 26 | -0.31 | 0.677 | 0.337 |
| I104 | 053515.55-050145.3 | 34 | -0.53 | 1.093 | 0.525 |
| I105 | 053515.59-050934.0 | 21 | -0.33 | 0.590 | 0.277 |
| I106 | 053515.61-045929.1 | 151 | -0.30 | 1.899 | 1.092 |
| I107 | 053515.65-045714.5 | 159 | -0.47 | 0.767 | 0.315 |
| I108 | 053515.76-051229.2 | 72 | 0.06 | ··· | ··· |
| I109 | 053515.80-050327.8 | 177 | -0.92 | 0.579 | 0.339 |
| I110 | 053515.93-051501.3 | 3013 | 0.20 | ··· | ··· |
| I111 | 053516.14-050921.1 | 88 | -0.91 | 0.622 | 0.234 |
| I112 | 053516.35-050438.1 | 17 | -0.76 | 0.561 | 0.329 |
| I113 | 053516.40-045803.7 | 264 | -0.79 | 0.605 | 0.161 |
| I114 | 053516.49-050332.0 | 294 | -0.80 | 0.655 | 0.197 |
| I115 | 053516.66-050856.2 | 4 | 0.50 | ··· | ··· |
| I116 | 053516.80-050729.2 | 45 | -0.91 | 0.490 | 0.341 |
| I117 | 053516.86-050749.5 | 16 | -0.62 | 0.995 | 0.540 |
| I118 | 053517.12-051240.9 | 74 | -0.54 | ··· | ··· |
| I119 | 053517.25-050317.7 | 10 | 0.80 | ··· | ··· |
| I120 | 053517.36-051231.1 | 65 | -0.66 | ··· | ··· |
| I121 | 053517.41-045958.4 | 259 | 0.20 | ··· | 1.775 |
| I122 | 053517.46-050950.9 | 44 | -1.00 | 0.578 | 0.299 |
| I123 | 053517.72-050032.1 | 29 | -0.17 | 2.217 | 1.373 |
| I124 | 053517.92-051535.0 | 830 | -0.14 | ··· | ··· |
| I125 | 053518.24-051308.9 | 561 | -0.40 | ··· | ··· |
| I126 | 053518.24-050355.9 | 92 | -1.00 | 0.041 | 0.013 |
| I127 | 053518.26-050806.9 | 7 | -0.14 | ··· | 1.263 |
| I128 | 053518.31-050034.8 | 60 | 0.93 | ··· | ··· |

TABLE 1—*Continued*

| ID[b] | Name[c] | X-ray[d] Counts | Hardness[e] Ratio | $J$–$H$[f] (mag) | $H$–$K$[f] (mag) |
|---|---|---|---|---|---|
| I129 | 053518.45-050832.7 | 15 | -0.73 | 0.595 | 0.235 |
| I130 | 053518.61-045944.0 | 165 | -0.71 | 0.583 | 0.201 |
| I131 | 053518.84-051448.1 | 661 | -0.48 | ··· | ··· |
| I132 | 053518.93-050051.9 | 23 | 0.65 | ··· | ··· |
| I133 | 053518.94-050638.1 | 26 | 0.85 | ··· | ··· |
| I134 | 053518.96-050324.9 | 7 | 1.00 | ··· | ··· |
| I135 | 053518.98-050031.0 | 24 | 0.83 | ··· | ··· |
| I136 | 053519.65-050230.4 | 11 | -0.82 | 0.647 | 0.307 |
| I137 | 053519.75-050533.4 | 6 | 0.67 | ··· | ··· |
| I138 | 053519.75-051536.7 | 359 | 0.67 | ··· | ··· |
| I139 | 053519.86-051510.2 | 309 | 0.25 | 1.610 | 1.034 |
| I140 | 053519.97-050104.1 | 259 | 0.83 | ··· | ··· |
| I141 | 053519.98-051405.6 | 202 | 0.03 | ··· | ··· |
| I142 | 053519.99-051252.9 | 97 | 0.86 | 2.063 | 1.310 |
| I143 | 053520.08-051318.8 | 1099 | 0.06 | ··· | ··· |
| I144 | 053520.14-051317.3 | 953 | 0.05 | 1.923 | 1.308 |
| I145 | 053520.37-050228.2 | 73 | -0.86 | 0.765 | 0.203 |
| I146 | 053520.59-050302.0 | 7 | 0.43 | ··· | 2.444 |
| I147 | 053520.74-051551.3 | 2276 | -0.12 | 1.177 | 0.558 |
| I148 | 053520.76-045835.6 | 673 | -0.37 | 1.118 | 0.463 |
| I149 | 053521.13-050634.2 | 109 | 0.63 | ··· | ··· |
| I150 | 053521.26-050918.2 | 2202 | -0.81 | 0.547 | 0.489 |
| I151 | 053521.31-051214.9 | 14667 | -0.63 | 0.604 | 0.176 |
| I152 | 053521.39-050944.2 | 29 | -0.79 | 0.686 | 0.490 |
| I153 | 053521.44-050905.6 | 142 | -0.62 | ··· | ··· |
| I154 | 053521.50-050155.3 | 97 | 0.13 | ··· | 2.056 |
| I155 | 053521.56-050941.0 | 76 | 0.84 | 0.837 | 0.715 |
| I156 | 053521.57-050951.7 | 260 | -0.64 | 0.784 | 0.528 |
| I157 | 053521.86-045650.5 | 93 | 0.08 | ··· | ··· |
| I158 | 053521.87-050703.7 | 838 | -0.71 | 0.950 | 0.558 |
| I159 | 053521.91-045919.5 | 15 | -0.20 | ··· | ··· |
| I160 | 053521.92-050352.4 | 8 | 0.25 | ··· | ··· |
| I161 | 053521.94-051430.1 | 345 | -0.69 | 0.747 | 0.226 |
| I162 | 053522.11-051507.7 | 479 | -0.32 | ··· | ··· |
| I163 | 053522.34-045954.7 | 23 | 0.65 | ··· | ··· |
| I164 | 053522.35-050741.0 | 507 | 0.02 | 2.624 | 1.649 |
| I165 | 053522.40-050807.0 | 833 | 0.21 | 1.396 | 0.873 |
| I166 | 053522.45-050913.0 | 415 | -0.92 | 0.583 | 0.124 |
| I167 | 053522.55-050802.6 | 921 | -0.34 | 1.412 | 0.531 |
| I168 | 053522.67-051413.8 | 206 | -0.69 | 0.903 | 0.519 |
| I169 | 053523.13-050037.7 | 13 | -0.08 | ··· | ··· |
| I170 | 053523.20-051345.6 | 164 | 0.04 | 1.756 | 0.742 |
| I171 | 053523.22-050845.8 | 13 | -0.38 | ··· | 1.935 |
| I172 | 053523.33-045722.3 | 182 | -0.63 | ··· | ··· |
| I173 | 053523.33-050823.5 | 59 | 0.19 | ··· | 2.256 |
| I174 | 053523.44-051053.9 | 1909 | -0.82 | 0.628 | 0.250 |
| I175 | 053523.51-050715.6 | 33 | 0.76 | ··· | ··· |
| I176 | 053523.53-051525.9 | 96 | -0.25 | ··· | ··· |
| I177 | 053524.34-050122.2 | 277 | 0.58 | ··· | ··· |
| I178 | 053524.58-051131.5 | 83 | -0.25 | 1.231 | 0.672 |
| I179 | 053524.61-051200.7 | 363 | -0.81 | 0.767 | 0.505 |
| I180 | 053524.66-050929.4 | 9 | 0.56 | ··· | 1.670 |
| I181 | 053524.87-050623.1 | 144 | 0.68 | 2.994 | 1.855 |
| I182 | 053525.03-050911.4 | 26 | -0.85 | 0.629 | 0.321 |
| I183 | 053525.07-051025.3 | 22 | 0.82 | 1.963 | 1.867 |
| I184 | 053525.17-050510.9 | 12 | 0.00 | ··· | ··· |
| I185 | 053525.17-051540.6 | 162 | -0.06 | ··· | ··· |
| I186 | 053525.22-050825.6 | 66 | 0.94 | ··· | ··· |
| I187 | 053525.24-050929.4 | 544 | -0.86 | 0.689 | 0.227 |
| I188 | 053525.36-050722.1 | 4 | 0.50 | ··· | ··· |
| I189 | 053525.40-051050.1 | 762 | -0.83 | 0.600 | 0.128 |
| I190 | 053525.44-050654.1 | 6 | 1.00 | ··· | ··· |
| I191 | 053525.53-045724.6 | 145 | 0.10 | ··· | ··· |
| I192 | 053525.64-050759.2 | 324 | -0.64 | 0.659 | 0.888 |

TABLE 1—*Continued*

| ID[b] | Name[c] | X-ray[d] Counts | Hardness[e] Ratio | $J$–$H$[f] (mag) | $H$–$K$[f] (mag) |
|---|---|---|---|---|---|
| I193 | 053525.72-050705.2 | 5 | -1.00 | 0.646 | 0.283 |
| I194 | 053525.73-050951.5 | 1411 | -0.68 | 0.615 | 0.335 |
| I195 | 053525.77-050559.7 | 9 | 0.11 | ··· | ··· |
| I196 | 053525.85-050247.0 | 5 | 1.00 | ··· | ··· |
| I197 | 053525.86-050758.3 | 878 | -0.79 | 1.027 | ··· |
| I198 | 053526.05-050839.7 | 83 | -0.76 | 0.586 | ··· |
| I199 | 053526.27-050742.9 | 8 | 1.00 | ··· | ··· |
| I200 | 053526.29-050841.9 | 3840 | -0.84 | 0.504 | 0.224 |
| I201 | 053526.34-051613.8 | 231 | -0.06 | 1.455 | 0.764 |
| I202 | 053526.47-045953.8 | 88 | 0.20 | ··· | 1.206 |
| I203 | 053526.66-050611.9 | 11 | 1.00 | ··· | ··· |
| I204 | 053526.85-051109.7 | 289 | 0.13 | 1.039 | 0.766 |
| I205 | 053527.07-050623.5 | 12 | 0.67 | ··· | ··· |
| I206 | 053527.15-051547.1 | 196 | -0.08 | 0.887 | 0.512 |
| I207 | 053527.41-050905.8 | 18 | -0.89 | 0.768 | 0.453 |
| I208 | 053527.45-050243.9 | 270 | 0.16 | ··· | 2.101 |
| I209 | 053527.63-050938.6 | 24 | 0.42 | 2.435 | 1.499 |
| I210 | 053527.73-051357.4 | 55 | 0.60 | 1.285 | 0.657 |
| I211 | 053527.79-051704.7 | 711 | -0.46 | ··· | ··· |
| I212 | 053527.83-050537.9 | 345 | 0.57 | ··· | ··· |
| I213 | 053528.06-050136.6 | 326 | 0.42 | ··· | 2.365 |
| I214 | 053528.14-051015.3 | 37 | -0.41 | 0.997 | 0.662 |
| I215 | 053528.18-050342.7 | 41 | 0.41 | ··· | ··· |
| I216 | 053528.19-050051.0 | 172 | -0.79 | 0.651 | 0.221 |
| I217 | 053528.21-051139.0 | 50 | -0.28 | 1.059 | 0.515 |
| I218 | 053528.27-045839.8 | 1228 | 0.61 | ··· | 2.812 |
| I219 | 053528.50-050748.6 | 89 | 0.03 | ··· | 2.158 |
| I220 | 053528.60-050546.0 | 28 | 0.29 | 2.581 | 1.501 |
| I221 | 053528.67-050307.9 | 8 | 0.50 | ··· | ··· |
| I222 | 053528.71-050553.0 | 11 | 0.82 | ··· | ··· |
| I223 | 053529.02-050605.6 | 1424 | -0.82 | 0.582 | 0.171 |
| I224 | 053529.25-050807.1 | 6 | 0.67 | ··· | ··· |
| I225 | 053529.45-051635.3 | 1189 | -0.53 | 0.864 | 0.257 |
| I226 | 053529.81-051609.4 | 476 | -0.63 | 0.780 | 0.311 |
| I227 | 053529.89-051212.4 | 136 | -0.78 | 0.646 | 0.200 |
| I228 | 053529.90-050428.5 | 8 | 1.00 | ··· | ··· |
| I229 | 053530.00-051229.5 | 157 | -0.61 | 0.705 | 0.487 |
| I230 | 053530.11-050911.3 | 23 | -0.74 | 0.602 | 0.266 |
| I231 | 053530.13-051420.8 | 148 | -0.27 | 1.180 | 0.607 |
| I232 | 053530.32-051353.8 | 213 | -0.10 | 1.612 | 0.849 |
| I233 | 053530.55-050335.7 | 13 | -0.08 | ··· | ··· |
| I234 | 053530.64-045937.4 | 222 | -0.34 | 2.291 | 1.522 |
| I235 | 053530.72-050647.1 | 6 | 0.33 | ··· | ··· |
| I236 | 053530.86-045814.2 | 67 | 0.25 | ··· | 1.693 |
| I237 | 053531.06-050416.0 | 91 | -0.93 | 0.571 | 0.115 |
| I238 | 053531.22-051230.1 | 311 | -0.80 | 0.660 | 0.231 |
| I239 | 053531.27-051203.6 | 82 | -0.41 | 0.620 | 0.299 |
| I240 | 053531.31-051535.1 | 2773 | -0.64 | 0.777 | 0.315 |
| I241 | 053531.46-050547.3 | 22 | 0.91 | ··· | ··· |
| I242 | 053531.48-051605.0 | 660 | -0.78 | 0.226 | 0.050 |
| I243 | 053531.49-050503.2 | 187 | -0.80 | 0.688 | 0.477 |
| I244 | 053531.57-050548.9 | 13 | 0.85 | 2.003 | 1.424 |
| I245 | 053531.58-051658.2 | 181 | -0.28 | 1.168 | 0.504 |
| I246 | 053531.61-050015.8 | 63 | 0.49 | 2.628 | 1.639 |
| I247 | 053531.91-050551.1 | 33 | 0.39 | ··· | ··· |
| I248 | 053531.96-050929.7 | 2062 | -0.65 | 0.812 | 0.414 |
| I249 | 053532.02-050807.0 | 7 | -0.14 | 1.046 | 0.618 |
| I250 | 053532.24-051200.1 | 38 | -0.53 | 0.746 | 0.484 |
| I251 | 053532.31-051145.8 | 175 | 0.29 | 2.176 | 1.141 |
| I252 | 053532.35-051428.1 | 150 | -0.45 | 0.982 | 0.356 |
| I253 | 053532.35-050831.6 | 25 | 0.76 | ··· | ··· |
| I254 | 053532.51-050211.7 | 14 | -0.71 | 0.599 | 0.193 |
| I255 | 053532.80-050753.4 | 23 | 0.65 | ··· | ··· |
| I256 | 053532.86-051606.4 | 1143 | -0.39 | 1.093 | 0.302 |

TABLE 1—*Continued*

| ID[b] | Name[c] | X-ray[d] Counts | Hardness[e] Ratio | $J$–$H$[f] (mag) | $H$–$K$[f] (mag) |
|---|---|---|---|---|---|
| I257 | 053532.97-051207.7 | 25 | 0.12 | 2.036 | 1.154 |
| I258 | 053533.00-051734.1 | 406 | -0.63 | 0.619 | 0.271 |
| I259 | 053533.16-051412.9 | 974 | -0.14 | 0.783 | 0.399 |
| I260 | 053533.38-050803.8 | 11 | 0.82 | ··· | ··· |
| I261 | 053533.52-051521.1 | 646 | -0.11 | ··· | ··· |
| I262 | 053533.61-050043.5 | 128 | -0.83 | 0.652 | 0.200 |
| I263 | 053533.64-050309.5 | 223 | -0.35 | 1.451 | 0.693 |
| I264 | 053533.83-050429.0 | 346 | 0.88 | 1.934 | 1.264 |
| I265 | 053533.86-050907.4 | 20 | -0.80 | 0.586 | 0.264 |
| I266 | 053534.26-045954.5 | 53 | 0.89 | ··· | ··· |
| I267 | 053534.48-051309.1 | 76 | -0.61 | 0.583 | 0.161 |
| I268 | 053534.52-050053.6 | 27 | 0.48 | 2.309 | 2.173 |
| I269 | 053534.68-051555.1 | 330 | -0.67 | 0.556 | 0.550 |
| I270 | 053535.11-051449.0 | 99 | 0.33 | ··· | ··· |
| I271 | 053535.12-050600.0 | 13 | 1.00 | ··· | ··· |
| I272 | 053535.36-051113.6 | 506 | -0.72 | 0.577 | 0.217 |
| I273 | 053535.48-050722.0 | 27 | 0.93 | ··· | ··· |
| I274 | 053535.55-050700.3 | 210 | -0.90 | 0.628 | 0.208 |
| I275 | 053535.63-050150.3 | 66 | 0.91 | ··· | ··· |
| I276 | 053535.64-051051.8 | 22 | -0.55 | 0.517 | 0.351 |
| I277 | 053535.71-051545.1 | 204 | -0.26 | 0.678 | 0.284 |
| I278 | 053536.02-051226.9 | 270 | -0.61 | 1.551 | 1.042 |
| I279 | 053536.19-050457.6 | 114 | 0.60 | 1.349 | 0.722 |
| I280 | 053536.40-050117.0 | 943 | -0.46 | 0.836 | 0.467 |
| I281 | 053536.51-050524.1 | 9 | 0.33 | ··· | ··· |
| I282 | 053536.56-050440.9 | 909 | -0.92 | 0.654 | 0.193 |
| I283 | 053536.69-050415.8 | 2221 | -0.67 | 0.746 | 0.315 |
| I284 | 053536.77-051000.9 | 11 | -0.45 | 0.796 | 0.557 |
| I285 | 053536.86-050734.2 | 10 | 0.60 | ··· | ··· |
| I286 | 053536.95-050527.6 | 24 | -0.33 | 0.508 | 0.432 |
| I287 | 053537.17-051031.4 | 312 | -0.88 | 0.677 | 0.268 |
| I288 | 053537.57-050449.2 | 16 | 0.12 | ··· | 1.505 |
| I289 | 053537.70-050633.6 | 298 | -0.64 | 0.668 | 0.283 |
| I290 | 053538.04-051510.1 | 122 | 0.48 | ··· | ··· |
| I291 | 053538.07-050318.9 | 13 | 0.38 | ··· | ··· |
| I292 | 053538.30-051420.9 | 246 | -0.42 | 0.750 | 0.223 |
| I293 | 053538.52-045942.0 | 518 | -0.31 | ··· | ··· |
| I294 | 053538.57-050805.2 | 75 | 0.12 | 2.532 | 1.365 |
| I295 | 053538.65-050958.6 | 320 | -0.72 | 0.578 | 0.303 |
| I296 | 053538.75-050457.1 | 40 | -0.55 | 1.936 | 1.035 |
| I297 | 053538.88-051244.0 | 1047 | -0.26 | 1.110 | 0.661 |
| I298 | 053539.04-050705.8 | 279 | -0.84 | 0.559 | 0.291 |
| I299 | 053539.08-050858.2 | 198 | -0.80 | 0.664 | 0.163 |
| I300 | 053539.17-050541.8 | 7 | 0.14 | ··· | ··· |
| I301 | 053539.39-050509.5 | 113 | 0.59 | ··· | ··· |
| I302 | 053539.72-045920.2 | 65 | 0.35 | ··· | ··· |
| I303 | 053539.97-050638.3 | 75 | -0.68 | 1.134 | 0.606 |
| I304 | 053540.19-050429.1 | 9 | 0.33 | ··· | ··· |
| I305 | 053540.47-050420.5 | 19 | 0.58 | ··· | ··· |
| I306 | 053540.59-051221.6 | 85 | -0.13 | 0.690 | 0.270 |
| I307 | 053540.66-051111.8 | 76 | 0.11 | 0.654 | 0.289 |
| I308 | 053540.80-050902.9 | 825 | -0.61 | 0.903 | 0.305 |
| I309 | 053541.04-050626.7 | 119 | -0.76 | 0.619 | 0.302 |
| I310 | 053541.38-050354.4 | 38 | -0.58 | 1.173 | 0.491 |
| I311 | 053541.72-050330.1 | 61 | -0.74 | 0.612 | 0.198 |
| I312 | 053541.81-050520.9 | 15 | -0.33 | 1.702 | 0.827 |
| I313 | 053542.04-051013.8 | 660 | -0.32 | 1.329 | 0.617 |
| I314 | 053542.04-051301.8 | 617 | -0.73 | 0.559 | 0.288 |
| I315 | 053542.40-051104.3 | 56 | 0.32 | ··· | ··· |
| I316 | 053542.64-045957.2 | 79 | 0.34 | ··· | ··· |
| I317 | 053542.78-051156.9 | 658 | -0.79 | 0.704 | 0.158 |
| I318 | 053542.98-050307.1 | 42 | -0.33 | 0.644 | 0.274 |
| I319 | 053543.27-050918.6 | 2262 | -0.79 | 0.682 | 0.169 |
| I320 | 053543.54-050542.0 | 48 | -0.08 | 0.874 | 0.689 |

TABLE 1—*Continued*

| ID[b] | Name[c] | X-ray[d] Counts | Hardness[e] Ratio | $J$–$H$[f] (mag) | $H$–$K$[f] (mag) |
|---|---|---|---|---|---|
| I321 | 053543.82-051001.6 | 174 | -0.67 | 0.597 | 0.268 |
| I322 | 053544.52-050733.2 | 288 | -0.87 | 0.705 | 0.200 |
| I323 | 053544.54-050006.7 | 45 | 0.24 | ··· | ··· |
| I324 | 053544.88-050718.5 | 5273 | -0.70 | 0.630 | 0.247 |
| I325 | 053545.70-050646.5 | 74 | 0.51 | ··· | ··· |
| I326 | 053546.10-051054.2 | 695 | -0.76 | 0.776 | 0.407 |
| I327 | 053547.25-050251.9 | 64 | 0.41 | ··· | ··· |
| I328 | 053547.77-051033.0 | 3604 | -0.81 | 0.542 | 0.212 |
| I329 | 053548.26-051117.3 | 60 | 0.07 | ··· | ··· |
| I330 | 053548.39-050522.4 | 67 | 0.55 | ··· | ··· |
| I331 | 053548.40-050129.7 | 193 | -0.60 | 0.928 | 0.680 |
| I332 | 053548.88-050033.4 | 88 | -0.45 | 0.968 | 0.271 |
| I333 | 053549.00-050544.0 | 31 | 0.10 | ··· | ··· |
| I334 | 053549.04-050142.4 | 288 | -0.49 | 0.771 | 0.355 |
| I335 | 053549.21-050225.0 | 49 | 0.55 | ··· | ··· |
| I336 | 053549.96-050426.2 | 88 | 0.39 | ··· | ··· |
| I337 | 053550.07-051024.0 | 63 | -0.33 | ··· | ··· |
| I338 | 053550.51-050226.5 | 63 | 0.27 | ··· | ··· |
| I339 | 053551.12-050710.5 | 1348 | -0.78 | 0.736 | 0.372 |
| I340 | 053551.46-050205.5 | 167 | 0.46 | ··· | ··· |
| I341 | 053551.61-050600.5 | 48 | 0.25 | ··· | ··· |
| I342 | 053551.66-050810.8 | 7972 | -0.73 | 0.625 | 0.143 |
| I343 | 053552.66-050507.0 | 4600 | -0.75 | 0.579 | 0.373 |
| I344 | 053553.71-050235.6 | 164 | -0.07 | 1.037 | 0.347 |
| I345 | 053553.86-050656.1 | 258 | 0.34 | ··· | ··· |
| I346 | 053554.05-050416.3 | 1398 | -0.81 | 0.867 | 0.489 |
| I347 | 053554.22-050545.0 | 74 | -0.03 | 0.654 | 0.204 |
| I348 | 053554.67-050630.3 | 168 | -0.56 | 0.554 | 0.301 |
| I349 | 053555.86-050444.3 | 87 | 0.24 | ··· | ··· |
| I350 | 053557.79-050504.6 | 169 | 0.14 | ··· | ··· |
| I351 | 053600.05-050434.0 | 134 | -0.27 | 0.574 | 0.406 |
| I352 | 053600.36-050552.3 | 68 | 0.06 | ··· | ··· |
| I353 | 053600.55-050505.3 | 413 | -0.27 | ··· | ··· |
| I354 | 053604.60-050402.3 | 250 | 0.10 | ··· | ··· |
| I355 | 053454.47-050414.3 | 18 | 0.67 | ··· | ··· |
| I356 | 053457.03-050252.0 | 6 | 1.00 | ··· | ··· |
| I357 | 053508.43-051226.3 | 34 | 0.47 | ··· | ··· |
| I358 | 053513.13-050753.3 | 4 | 1.00 | ··· | ··· |
| I359 | 053518.87-050953.2 | 5 | 1.00 | ··· | ··· |
| I360 | 053521.33-051248.1 | 15 | 0.47 | ··· | ··· |
| I361 | 053521.50-050727.8 | 4 | 1.00 | ··· | ··· |
| I362 | 053522.42-050242.4 | 4 | 1.00 | ··· | ··· |
| I363 | 053522.67-050651.3 | 3 | 1.00 | ··· | ··· |
| I364 | 053529.78-045955.7 | 27 | 0.63 | ··· | ··· |
| I365 | 053530.67-050411.7 | 4 | 1.00 | ··· | ··· |
| I366 | 053531.19-050917.5 | 8 | 1.00 | ··· | ··· |
| I367 | 053533.14-051510.5 | 268 | 0.26 | ··· | ··· |
| I368 | 053547.84-050823.3 | 28 | 0.57 | ··· | ··· |
| I369 | 053550.91-050106.7 | 91 | 0.45 | ··· | ··· |
| I370 | 053444.08-050600.1 | 57 | 0.30 | ··· | ··· |
| I371 | 053452.91-050805.0 | 18 | 0.00 | ··· | ··· |
| I372 | 053500.97-050541.4 | 8 | -0.75 | 0.410 | 0.346 |
| I373 | 053507.89-050905.3 | 3 | -1.00 | ··· | ··· |
| I374 | 053510.79-051045.3 | 3 | -1.00 | ··· | ··· |
| I375 | 053514.97-050444.9 | 3 | -1.00 | ··· | ··· |
| I376 | 053519.73-051145.3 | 34 | 0.00 | ··· | ··· |
| I377 | 053529.82-051330.9 | 49 | 0.18 | ··· | ··· |
| I378 | 053530.76-050337.3 | 5 | -1.00 | ··· | ··· |
| I379 | 053533.75-045928.7 | 15 | -0.07 | ··· | ··· |
| I380 | 053535.70-050909.1 | 6 | -0.33 | ··· | ··· |
| I381 | 053538.44-051010.5 | 28 | -0.50 | 0.608 | 0.314 |
| I382 | 053542.37-050252.1 | 15 | -0.60 | ··· | ··· |
| I383 | 053544.67-050040.4 | 31 | -0.55 | 0.754 | 0.347 |
| I384 | 053546.94-050700.7 | 14 | -0.29 | ··· | ··· |

TABLE 1—*Continued*

| ID[b] | Name[c] | X-ray[d] Counts | Hardness[e] Ratio | $J$–$H$[f] (mag) | $H$–$K$[f] (mag) |
|---|---|---|---|---|---|
| I385 | 053554.84-050527.6 | 23 | -0.30 | ··· | ··· |
| S1 | 053554.73-045808.9 | 2987 | -0.87 | 0.483 | 0.168 |
| S2 | 053556.14-045657.7 | 1681 | -0.75 | 0.616 | 0.189 |
| S3 | 053556.28-045505.9 | 510 | 0.13 | ··· | ··· |
| S4 | 053558.84-045537.0 | 799 | 0.03 | ··· | 0.808 |
| S5 | 053559.31-045846.1 | 743 | -0.64 | 0.695 | 0.162 |
| S6 | 053602.99-045736.2 | 304 | -0.30 | ··· | ··· |
| S7 | 053604.24-045744.3 | 285 | -0.25 | ··· | ··· |
| S8 | 053605.75-045110.3 | 832 | -0.39 | ··· | ··· |
| S9 | 053611.84-050032.2 | 567 | -0.47 | 0.690 | 0.168 |
| S10 | 053612.81-045515.5 | 462 | -0.29 | ··· | ··· |
| S11 | 053628.11-045709.3 | 185 | 0.43 | ··· | ··· |
| S12 | 053614.94-045707.7 | 72 | 0.47 | ··· | ··· |
| S13 | 053620.26-045424.0 | 164 | 0.34 | ··· | ··· |

[a]Results of X-ray imaging analysis and 2MASS correlation are listed for all the detected X-ray sources.

[b]I1–I354 and S1–S11 are detected in the total band image (0.5–8.0 keV) image of the ACIS-I and the ACIS-S2. I355–I369 and S12–S13 are detected only in the hard band (2.0–8.0 keV) image of the ACIS-I and the ACIS-S2. I370–I385 are detected only in the soft band (0.5–2.0 keV) image of the ACIS-I. No new source was detected in the soft band image of the ACIS-S2.

[c]Sources are named after their position in the equinox J2000

[d]X-ray photon counts in 0.5–8.0 keV band.

[e]Defined as $H - S/H + S$ where $H$ and $S$ are photon counts in the hard band (2.0–8.0 keV) and in the soft band (0.5–2.0 keV) respectively.

[f]$J$–$H$ and $H$–$K$ in CIT color system derived from 2MASS $J$, $H$, and $K_s$-band photometry and Carpenter (2001).

TABLE 2

RESULTS OF TIMING AND SPECTROSCOPIC ANALYSIS[a]

| ID[b] | Upper[c] Probability | $N_{\rm H}$[d] ($10^{22}$ cm$^{-2}$) | $k_BT$[de] (keV) | Metallicity[deg] (solar) | $L_X$[df] ($10^{29}$ erg s$^{-1}$) | Class[h] |
|---|---|---|---|---|---|---|
| I4† | 0.005 | 0.14 (0.12–0.16) | 1.40 (1.29–1.60) | 0.10 (0.07–0.12) | 6.90 (6.50–7.31) | III+MS |
| I6† | 0.000 | 0.07 (0.05–0.08) | 0.99 (0.94–1.04) | 0.10 (0.09–0.12) | 7.64 (7.28–8.01) | III+MS |
| I7 | 0.014 | 0.14 (0.13–0.16) | 0.85 (0.81–0.88) | 0.07 (0.06–0.08) | 9.95 (9.50–10.41) | III+MS |
| I10 | 0.008 | 0.07 (0.05–0.08) | 0.98 (0.94–1.02) | 0.13 (0.12–0.14) | 11.51 (11.07–11.96) | III+MS |
| I12 | 0.196 | 0.14 (0.12–0.16) | 1.25 (1.16–1.34) | 0.13 (0.11–0.15) | 6.62 (6.24–6.99) | III+MS |
| I13† | 0.000 | 0.07 (0.06–0.07) | 1.09 (1.06–1.13) | 0.03 (0.02–0.03) | 27.49 (26.78–28.19) | other |
| I14 | 0.079 | 0.02 (0.01–0.04) | 1.11 (1.06–1.34) | 0.08 (0.07–0.10) | 8.14 (7.78–8.50) | III+MS |
| I17 | 0.245 | 0.05 (0.04–0.07) | 1.02 (0.96–1.07) | 0.07 (0.06–0.08) | 8.28 (7.91–8.66) | III+MS |
| I20† | 0.000 | 0.12 (0.10–0.14) | 0.80 (0.76–0.84) | 0.12 (0.10–0.13) | 5.37 (5.04–5.69) | III+MS |
| I21 | 0.226 | 0.00 (0.00–0.01) | 1.06 (1.00–1.12) | 0.14 (0.12–0.16) | 3.56 (3.34–3.78) | III+MS |
| I25† | 0.013 | 0.05 (0.05–0.06) | 1.05 (1.02–1.07) | 0.14 (0.13–0.15) | 35.16 (34.41–35.92) | other |
| I27 | 0.266 | 0.17 (0.16–0.19) | 1.31 (1.25–1.37) | 0.26 (0.24–0.29) | 10.69 (10.22–11.17) | III+MS |
| I28 | 0.015 | 0.00 (0.00–0.02) | 1.26 (1.14–1.38) | 0.16 (0.13–0.19) | 3.10 (2.88–3.32) | III+MS |
| I31 | 0.110 | 0.32 (0.30–0.34) | 1.03 (1.00–1.07) | 0.12 (0.11–0.14) | 18.72 (18.01–19.43) | III+MS |
| I33 | 0.000 | 0.14 (0.11–0.18) | 0.85 (0.76–0.96) | 0.07 (0.05–0.09) | 1.90 (1.70–2.10) | III+MS |
| I36 | 0.124 | 0.03 (0.02–0.05) | 1.21 (1.16–1.26) | 0.36 (0.34–0.39) | 9.15 (8.79–9.51) | III+MS |
| I42† | 0.006 | 0.34 (0.33–0.36) | 1.63 (1.55–1.71) | 0.16 (0.14–0.18) | 28.50 (27.57–29.43) | II |
| I47† | 0.001 | 0.29 (0.28–0.31) | 1.65 (1.59–1.71) | 0.19 (0.17–0.21) | 43.22 (42.16–44.28) | III+MS |
| I51 | 0.000 | 0.19 (0.18–0.19) | 2.56 (2.52–2.59) | 0.38 (0.37–0.39) | 612.99 (609.09–616.87) | III+MS |
| I54 | 0.603 | 0.10 (0.08–0.12) | 1.22 (1.14–1.29) | 0.23 (0.21–0.26) | 7.16 (6.81–7.51) | III+MS |
| I56 | 0.058 | 0.06 (0.05–0.08) | 0.74 (0.69–0.79) | 0.11 (0.10–0.12) | 4.97 (4.68–5.26) | III+MS |
| I65† | 0.665 | 0.53 (0.48–0.59) | 3.35 (2.91–3.83) | 0.00 (-0.16–0.14) | 10.13 (9.44–10.81) | II |
| I67† | 0.813 | 0.88 (0.85–0.91) | 2.95 (2.83–3.14) | 1.60 (1.50–1.71) | 64.39 (62.53–66.26) | II |
| I71 | 0.001 | 0.00 (0.00–0.03) | 1.04 (1.02–1.07) | 0.20 (0.19–0.21) | 14.26 (13.84–14.69) | III+MS |
| I74 | 0.691 | 2.16 (2.07–2.25) | 2.31 (2.19–2.46) | 0.28 (0.18–0.37) | 45.76 (43.47–48.02) | I |
| I77 | 0.240 | 3.31 (3.21–3.41) | 2.91 (2.79–3.07) | 0.74 (0.65–0.85) | 116.03 (111.84–120.22) | I |
| I82 | 0.177 | 3.92 (3.70–4.16) | 2.24 (2.01–2.56) | 4.03 (3.60–4.46) | 49.90 (46.16–53.67) | ··· |
| I85† | 0.026 | 0.01 (0.00–0.03) | 1.63 (1.55–1.70) | 0.35 (0.32–0.38) | 33.26 (32.23–34.31) | III+MS |
| I87 | 0.788 | 2.57 (2.44–2.72) | 1.68 (1.53–1.83) | 2.44 (2.17–2.71) | 32.89 (30.30–35.48) | I |
| I89 | 0.000 | 1.01 (0.89–1.15) | 7.05 (4.97–12.32) | 0.26 (-0.20–0.72) | 11.65 (10.59–12.71) | I |
| I92 | 0.193 | 0.07 (0.05–0.09) | 0.98 (0.92–1.05) | 0.15 (0.13–0.17) | 4.48 (4.22–4.75) | ··· |
| I93† | 0.856 | 0.07 (0.05–0.08) | 0.84 (0.81–0.88) | 0.07 (0.07–0.08) | 8.54 (8.17–8.90) | III+MS |
| I96 | 0.262 | 1.90 (1.81–2.00) | 2.46 (2.31–2.61) | 0.01 (-0.09–0.11) | 28.04 (26.46–29.62) | I |
| I110† | 0.849 | 1.21 (1.18–1.24) | 7.61 (7.13–8.37) | 0.11 (0.03–0.19) | 209.63 (205.71–213.57) | ··· |
| I113 | 0.512 | 0.00 (0.00–0.03) | 0.82 (0.77–0.87) | 0.12 (0.11–0.14) | 3.28 (3.06–3.50) | III+MS |
| I114 | 0.124 | 0.08 (0.06–0.10) | 0.82 (0.78–0.87) | 0.23 (0.21–0.25) | 4.09 (3.84–4.33) | III+MS |
| I121 | 0.981 | 2.47 (2.36–2.60) | 1.93 (1.77–2.10) | 1.06 (0.92–1.21) | 34.47 (32.28–36.66) | I |
| I124† | 0.930 | 0.74 (0.71–0.79) | 3.52 (3.23–3.70) | 0.00 (-0.16–0.04) | 41.27 (39.16–42.37) | ··· |
| I125 | 0.430 | 0.54 (0.51–0.58) | 2.56 (2.33–2.79) | 0.62 (0.53–0.72) | 20.92 (19.99–21.85) | ··· |
| I131† | 0.461 | 0.23 (0.21–0.25) | 2.83 (2.56–3.18) | 0.25 (0.17–0.33) | 17.72 (16.98–18.48) | ··· |
| I138† | 0.441 | 3.60 (3.41–3.82) | 5.23 (4.65–5.84) | 0.00 (-0.25–0.24) | 48.11 (45.34–50.89) | I |
| I139 | 0.000 | 0.00 (0.00–0.00) | 3.56 (3.45–3.56) | 0.32 (-0.40–0.44) | 2.06 (1.82–2.30) | I |
| I140 | 0.400 | 5.88 (5.56–6.23) | 3.22 (2.92–3.52) | 1.20 (0.95–1.45) | 60.02 (56.14–63.90) | I |
| I141 | 0.041 | 0.33 (0.26–0.42) | 5.55 (3.71–9.64) | 0.55 (0.07–1.03) | 4.78 (4.27–5.29) | ··· |
| I143 | 0.352 | 1.68 (1.63–1.73) | 2.62 (2.50–2.74) | 0.44 (0.37–0.51) | 89.11 (86.28–91.92) | ··· |
| I144 | 0.363 | 1.51 (1.46–1.56) | 2.73 (2.62–2.84) | 0.00 (-0.06–0.07) | 70.64 (68.28–73.04) | I |
| I147† | 0.051 | 1.07 (1.05–1.10) | 2.66 (2.57–2.75) | 0.26 (0.22–0.30) | 138.00 (134.98–141.05) | II |
| I148† | 0.083 | 0.59 (0.56–0.62) | 2.39 (2.23–2.56) | 0.09 (0.04–0.15) | 26.85 (25.76–27.94) | II |
| I150† | 0.000 | 0.21 (0.20–0.22) | 0.95 (0.93–0.97) | 0.23 (0.22–0.24) | 42.64 (41.71–43.58) | other |
| I151 | 0.000 | 0.32 (0.32–0.32) | 1.67 (1.65–1.69) | 0.33 (0.32–0.34) | 395.08 (391.75–398.37) | III+MS |
| I156 | 0.005 | 0.08 (0.05–0.11) | 3.17 (2.74–3.67) | 1.63 (1.39–1.88) | 5.55 (5.18–5.91) | other |
| I158 | 0.256 | 0.27 (0.25–0.29) | 1.33 (1.28–1.39) | 0.22 (0.20–0.24) | 18.63 (17.97–19.28) | II |
| I161 | 0.195 | 0.12 (0.10–0.15) | 0.94 (0.88–1.00) | 0.14 (0.13–0.16) | 5.54 (5.20–5.87) | III+MS |
| I162 | 0.031 | 0.30 (0.26–0.33) | 2.01 (1.73–2.26) | 0.26 (0.19–0.33) | 9.63 (9.03–10.22) | ··· |
| I164† | 0.248 | 2.01 (1.94–2.08) | 2.00 (1.87–2.12) | 1.77 (1.64–1.91) | 48.96 (46.73–51.20) | I |
| I165† | 0.062 | 1.25 (1.20–1.31) | 5.76 (5.18–6.59) | 0.36 (0.18–0.53) | 51.96 (50.10–53.84) | II |
| I166 | 0.624 | 0.02 (0.00–0.04) | 0.94 (0.90–0.98) | 0.43 (0.40–0.46) | 5.36 (5.09–5.63) | III+MS |
| I167 | 0.295 | 0.69 (0.66–0.72) | 2.48 (2.32–2.63) | 0.65 (0.58–0.72) | 37.13 (35.89–38.38) | II |
| I168 | 0.803 | 0.26 (0.23–0.29) | 1.00 (0.93–1.07) | 0.17 (0.14–0.20) | 4.47 (4.12–4.82) | II |
| I174† | 0.009 | 0.00 (0.00–0.02) | 1.22 (1.19–1.26) | 0.22 (0.21–0.24) | 25.16 (24.56–25.75) | III+MS |
| I177† | 0.035 | 3.26 (3.09–3.46) | 3.49 (3.01–4.11) | 4.71 (4.22–5.20) | 40.79 (38.19–43.41) | ··· |
| I179 | 0.210 | 0.14 (0.12–0.16) | 0.75 (0.71–0.79) | 0.10 (0.09–0.11) | 7.46 (7.05–7.87) | other |
| I187 | 0.874 | 0.04 (0.03–0.06) | 1.03 (0.99–1.08) | 0.12 (0.11–0.14) | 8.21 (7.85–8.57) | III+MS |
| I189† | 0.002 | 0.00 (0.00–0.01) | 1.21 (1.15–1.27) | 0.16 (0.14–0.17) | 10.02 (9.64–10.40) | III+MS |

TABLE 2—*Continued*

| ID[b] | Upper[c] Probability | $N_{\rm H}$[d] ($10^{22}$ cm$^{-2}$) | $k_BT$[de] (keV) | Metallicity[deg] (solar) | $L_X$[df] ($10^{29}$ erg s$^{-1}$) | Class[h] |
|---|---|---|---|---|---|---|
| I192 | 0.038 | 0.16 (0.13–0.18) | 2.02 (1.66–2.26) | 0.41 (0.33–0.48) | 6.54 (6.16–6.91) | other |
| I194† | 0.016 | 0.22 (0.21–0.24) | 1.59 (1.53–1.65) | 0.33 (0.31–0.36) | 30.58 (29.74–31.42) | III+MS |
| I197† | 0.532 | 0.07 (0.06–0.08) | 1.22 (1.16–1.28) | 0.16 (0.15–0.18) | 13.41 (12.95–13.87) | other |
| I200† | 0.000 | 0.08 (0.08–0.09) | 0.96 (0.94–0.97) | 0.14 (0.14–0.15) | 58.62 (57.65–59.59) | III+MS |
| I204 | 0.371 | 1.83 (1.74–1.93) | 2.81 (2.58–3.12) | 4.67 (4.25–5.08) | 25.09 (23.53–26.63) | II |
| I208 | 0.688 | 1.74 (1.64–1.86) | 3.38 (3.02–3.74) | 0.00 (-0.17–0.16) | 22.07 (20.66–23.49) | I |
| I211 | 0.166 | 0.27 (0.25–0.30) | 1.99 (1.83–2.15) | 0.15 (0.11–0.20) | 25.29 (24.22–26.37) | ··· |
| I212† | 0.812 | 3.92 (3.77–4.11) | 2.07 (1.98–2.15) | 0.00 (-0.10–0.07) | 58.90 (55.25–61.84) | I |
| I213† | 0.243 | 3.04 (2.92–3.19) | 2.04 (1.93–2.13) | 0.00 (-0.09–0.07) | 46.47 (43.63–49.06) | I |
| I218† | 0.138 | 3.80 (3.71–3.90) | 2.71 (2.61–2.81) | 0.84 (0.76–0.92) | 212.30 (206.01–218.57) | I |
| I223† | 0.007 | 0.16 (0.15–0.17) | 1.03 (1.01–1.06) | 0.18 (0.17–0.20) | 24.54 (23.87–25.20) | III+MS |
| I225† | 0.002 | 0.19 (0.17–0.21) | 2.55 (2.37–2.74) | 0.23 (0.18–0.27) | 34.11 (33.03–35.19) | II |
| I226 | 0.198 | 0.24 (0.22–0.27) | 1.30 (1.23–1.36) | 0.19 (0.16–0.21) | 10.64 (10.10–11.18) | III+MS |
| I232 | 0.532 | 1.61 (1.51–1.71) | 1.79 (1.67–1.96) | 5.00 (4.51–5.50) | 16.06 (14.74–17.38) | I |
| I234 | 0.353 | 0.93 (0.87–1.01) | 1.47 (1.36–1.57) | 0.00 (-0.05–0.03) | 11.87 (10.93–12.66) | I |
| I238 | 0.267 | 0.04 (0.02–0.06) | 0.79 (0.75–0.84) | 0.10 (0.09–0.11) | 4.33 (4.06–4.59) | III+MS |
| I240 | 0.005 | 0.46 (0.45–0.47) | 1.27 (1.25–1.30) | 0.16 (0.15–0.17) | 94.24 (92.37–96.09) | III+MS |
| I242 | 0.004 | 0.23 (0.22–0.25) | 0.69 (0.67–0.71) | 0.18 (0.17–0.19) | 15.22 (14.57–15.87) | III+MS |
| I248† | 0.000 | 0.22 (0.21–0.23) | 1.60 (1.54–1.66) | 0.15 (0.13–0.16) | 44.82 (43.78–45.85) | III+MS |
| I256 | 0.545 | 0.37 (0.35–0.39) | 2.53 (2.38–2.67) | 0.02 (-0.02–0.06) | 36.72 (35.52–37.91) | other |
| I258 | 0.984 | 0.14 (0.11–0.16) | 0.94 (0.88–1.00) | 0.12 (0.10–0.13) | 6.46 (6.05–6.86) | III+MS |
| I259† | 0.147 | 0.29 (0.27–0.32) | 11.50 (9.17–14.33) | 0.28 (0.04–0.52) | 37.15 (35.88–38.41) | II |
| I261† | 0.318 | 0.59 (0.55–0.64) | 5.64 (4.87–6.63) | 0.00 (-0.23–0.12) | 27.28 (26.06–28.51) | ··· |
| I263 | 0.761 | 0.96 (0.90–1.03) | 1.50 (1.40–1.61) | 0.00 (-0.04–0.04) | 12.87 (11.97–13.76) | II |
| I264† | 0.160 | 5.74 (5.42–6.11) | 7.54 (6.11–10.43) | 1.64 (1.27–2.00) | 62.79 (59.27–66.33) | I |
| I269 | 0.892 | 0.15 (0.12–0.17) | 1.17 (1.06–1.26) | 0.14 (0.12–0.17) | 7.02 (6.58–7.45) | other |
| I272† | 0.041 | 0.08 (0.06–0.10) | 1.33 (1.26–1.41) | 0.13 (0.11–0.15) | 8.43 (8.04–8.83) | III+MS |
| I274 | 0.671 | 0.06 (0.04–0.08) | 0.95 (0.87–1.04) | 0.10 (0.08–0.12) | 3.13 (2.90–3.36) | III+MS |
| I277 | 0.040 | 0.19 (0.15–0.24) | 3.04 (2.63–4.01) | 1.57 (1.30–1.92) | 5.05 (4.61–5.49) | III+MS |
| I278 | 0.002 | 0.12 (0.10–0.15) | 0.79 (0.74–0.84) | 0.04 (0.03–0.05) | 4.30 (4.00–4.60) | I |
| I280† | 0.918 | 0.52 (0.49–0.54) | 2.50 (2.34–2.66) | 1.22 (1.13–1.31) | 36.72 (35.49–37.93) | II |
| I282 | 0.843 | 0.07 (0.06–0.08) | 0.93 (0.90–0.97) | 0.18 (0.17–0.20) | 13.49 (13.04–13.95) | III+MS |
| I283† | 0.000 | 0.10 (0.09–0.11) | 1.97 (1.88–2.06) | 0.46 (0.43–0.49) | 41.61 (40.70–42.53) | III+MS |
| I287 | 0.160 | 0.00 (0.00–0.04) | 0.82 (0.77–0.86) | 0.10 (0.09–0.11) | 4.00 (3.77–4.24) | III+MS |
| I289† | 0.410 | 0.08 (0.06–0.11) | 2.84 (2.44–3.42) | 0.41 (0.28–0.53) | 6.37 (5.99–6.75) | III+MS |
| I292 | 0.997 | 0.02 (0.00–0.05) | 1.25 (1.14–1.37) | 0.24 (0.19–0.28) | 2.55 (2.32–2.77) | III+MS |
| I293 | 0.894 | 0.54 (0.51–0.58) | 2.84 (2.60–3.14) | 0.12 (0.03–0.21) | 20.92 (19.95–21.90) | ··· |
| I295† | 0.179 | 0.18 (0.16–0.21) | 0.82 (0.78–0.87) | 0.08 (0.07–0.10) | 6.35 (5.97–6.72) | III+MS |
| I297† | 0.066 | 0.59 (0.56–0.62) | 3.20 (2.98–3.42) | 0.45 (0.37–0.53) | 43.61 (42.19–45.01) | II |
| I298 | 0.121 | 0.09 (0.07–0.11) | 0.77 (0.72–0.82) | 0.07 (0.06–0.07) | 4.35 (4.08–4.63) | III+MS |
| I308 | 0.081 | 0.38 (0.36–0.40) | 1.56 (1.48–1.64) | 0.18 (0.15–0.20) | 33.49 (32.28–34.71) | II |
| I313 | 0.239 | 0.61 (0.58–0.64) | 2.30 (2.18–2.45) | 0.04 (-0.01–0.09) | 26.76 (25.67–27.85) | II |
| I314 | 0.061 | 0.17 (0.15–0.19) | 1.00 (0.96–1.04) | 0.14 (0.13–0.15) | 11.75 (11.24–12.27) | III+MS |
| I317 | 0.504 | 0.10 (0.09–0.12) | 1.03 (0.99–1.06) | 0.13 (0.12–0.14) | 12.34 (11.83–12.85) | III+MS |
| I319† | 0.001 | 0.06 (0.06–0.07) | 1.23 (1.19–1.26) | 0.11 (0.10–0.12) | 36.51 (35.71–37.30) | III+MS |
| I322 | 0.566 | 0.04 (0.02–0.06) | 0.92 (0.84–0.98) | 0.17 (0.15–0.19) | 4.01 (3.76–4.25) | III+MS |
| I324† | 0.000 | 0.12 (0.11–0.12) | 1.61 (1.57–1.64) | 0.15 (0.14–0.16) | 105.68 (104.17–107.17) | III+MS |
| I326† | 0.003 | 0.10 (0.09–0.11) | 1.00 (0.96–1.05) | 0.09 (0.08–0.10) | 11.73 (11.25–12.20) | III+MS |
| I328 | 0.000 | 0.08 (0.07–0.09) | 1.17 (1.14–1.20) | 0.12 (0.11–0.13) | 63.15 (62.08–64.24) | III+MS |
| I334 | 0.028 | 0.04 (0.02–0.07) | 1.57 (1.28–1.77) | 0.26 (0.20–0.31) | 3.82 (3.54–4.09) | III+MS |
| I339† | 0.010 | 0.08 (0.07–0.09) | 1.23 (1.18–1.28) | 0.10 (0.09–0.11) | 23.32 (22.66–23.98) | III+MS |
| I342 | 0.000 | 0.13 (0.13–0.14) | 1.33 (1.31–1.35) | 0.09 (0.08–0.09) | 170.53 (168.58–172.51) | III+MS |
| I343† | 0.000 | 0.16 (0.15–0.16) | 1.27 (1.25–1.30) | 0.12 (0.12–0.13) | 94.26 (92.82–95.68) | other |
| I345 | 0.103 | 1.47 (1.29–1.68) | 10.10 (7.56–38.89) | 1.25 (0.74–2.07) | 14.26 (13.01–15.51) | ··· |
| I346 | 0.000 | 0.10 (0.09–0.11) | 0.98 (0.95–1.01) | 0.13 (0.12–0.13) | 23.55 (22.89–24.22) | II |
| I368 | 0.313 | 1.36 (1.24–1.52) | 9.85 (7.29–23.02) | 0.00 (-0.54–0.32) | 16.62 (15.30–17.76) | ··· |
| S1† | 0.360 | 0.08 (0.08–0.09) | 0.91 (0.89–0.93) | 0.34 (0.34–0.35) | 59.24 (58.12–60.38) | III+MS |
| S2 | 0.005 | 0.03 (0.02–0.04) | 0.95 (0.92–0.98) | 0.14 (0.13–0.15) | 21.79 (21.20–22.39) | III+MS |
| S5 | 0.391 | 0.32 (0.30–0.34) | 0.75 (0.72–0.79) | 0.19 (0.18–0.20) | 17.52 (16.75–18.29) | III+MS |

[a]Results of timing and spectroscopic analysis are listed for all the "bright2" sources. Best-fit parameters of thin-thermal plasma model fitting are tabulated regardless whether the fit is accepted or rejected.

[b]Sources with time-variability are shown with †.

[c]Defined as $\int_\alpha^\infty \chi^2_\nu(x)dx$ where the $\chi^2$-value and the degree of freedom of the fit is $\alpha$ and $\nu$. Fits with the upper probability larger than 0.01 are "accepted" while those less than or equal to 0.01 are "rejected". Even the "best-fit" parameters of rejected fittings represent values of some physical meaning or approximated values. We thus use these values in the same way with the accepted ones.

[d]The lower and upper boundary for 1 $\sigma$ confidence level are given in parentheses.

[e]The best fit value of temperature and metallicity are searched for in the range of less than 20 keV and 5 solar respectively.

[f]Luminosity in 0.5–8.0 keV band (corrected for absorption).

[g]Abundance relative to solar photospheric (Morrison & McCammon 1983).

[h]Classification based on the $J$, $H$, and $K_s$-band magnitude of 2MASS counterpart. "I" for class I, "II" for class II, and "III+MS" for class III+MS. "others" are for sources which are out of these groups. " ··· " sources can not be classified

TABLE 3

BEST-FIT VALUES OF TWO-TEMPERATURE THIN-THERMAL PLASMA MODEL[a]

| ID | $N_{\rm H}$[b] ($10^{22}$ cm$^{-2}$) | $k_BT_1$[bce] (keV) | $k_BT_2$[bde] (keV) | Metallicity[beg] (solar) | $L_{X1}$[bcf] ($10^{29}$ erg s$^{-1}$) | $L_{X2}$[bdf] ($10^{29}$ erg s$^{-1}$) | Class[g] |
|---|---|---|---|---|---|---|---|
| I10 | 0.42(0.41–0.44) | 0.22(0.21–0.22) | 1.07(1.02–1.12) | 0.43(0.41–0.45) | 33.08(30.39–35.88) | 12.31(11.62–13.00) | III+MS |
| I42 | 0.36(0.34–0.38) | 1.14(1.11–1.23) | 2.41(2.20–2.65) | 0.18(0.16–0.21) | 12.43(11.55–13.29) | 17.62(16.61–18.64) | II |
| I47 | 0.36(0.35–0.38) | 0.79(0.75–0.83) | 2.46(2.31–2.62) | 0.47(0.45–0.50) | 15.30(14.28–16.32) | 36.59(35.36–37.82) | III+MS |
| I71 | 0.00(0.00–0.02) | 0.80(0.77–0.83) | 2.08(1.92–2.25) | 0.78(0.75–0.82) | 6.64(6.28–7.00) | 9.18(8.68–9.69) | III+MS |
| I150 | 0.24(0.23–0.25) | 0.83(0.81–0.85) | 10.51(6.34–26.52) | 0.33(0.32–0.34) | 39.42(38.43–40.41) | 12.26(11.11–13.43) | other |
| I156 | 0.22(0.19–0.25) | 0.84(0.72–0.98) | 2.53(2.26–9.32) | 0.61(0.52–0.70) | 1.39(1.11–1.67) | 4.62(4.21–5.02) | other |
| I174 | 0.00(0.00–0.01) | 1.06(1.04–1.09) | 3.71(3.01–4.69) | 0.29(0.27–0.30) | 17.93(17.37–18.48) | 9.80(8.99–10.62) | III+MS |
| I189 | 0.00(0.00–0.01) | 0.59(0.52–0.65) | 1.70(1.61–1.79) | 0.55(0.51–0.59) | 2.51(2.23–2.79) | 8.04(7.64–8.44) | III+MS |
| I200 | 0.04(0.03–0.04) | 0.83(0.81–0.84) | 2.27(2.14–2.43) | 0.51(0.49–0.52) | 28.99(28.22–29.75) | 28.45(27.43–29.47) | III+MS |
| I223 | 0.13(0.12–0.14) | 0.79(0.75–0.82) | 1.75(1.67–1.82) | 0.64(0.61–0.67) | 9.72(9.17–10.28) | 14.57(13.90–15.23) | III+MS |
| I225 | 0.28(0.27–0.30) | 1.00(0.95–1.06) | 10.09(7.13–16.98) | 0.11(0.10–0.12) | 20.03(19.02–21.05) | 22.15(20.68–23.64) | II |
| I240 | 0.51(0.50–0.52) | 0.86(0.83–0.89) | 2.02(1.92–2.11) | 0.32(0.30–0.33) | 47.06(45.07–49.08) | 61.20(59.25–63.18) | III+MS |
| I242 | 0.15(0.13–0.16) | 0.70(0.67–0.73) | 2.44(1.95–3.28) | 0.69(0.65–0.72) | 8.76(8.28–9.25) | 3.99(3.46–4.52) | III+MS |
| I248 | 0.27(0.26–0.28) | 0.84(0.81–0.87) | 2.93(2.75–3.16) | 0.28(0.27–0.30) | 20.34(19.38–21.30) | 33.04(31.81–34.28) | III+MS |
| I278 | 0.01(0.00–0.04) | 0.71(0.65–0.79) | 3.17(2.67–12.51) | 0.40(0.34–0.47) | 1.15(0.97–1.32) | 3.03(2.71–3.36) | I |
| I283 | 0.11(0.10–0.12) | 0.89(0.85–0.94) | 2.89(2.75–3.11) | 0.96(0.92–1.00) | 7.99(7.39–8.59) | 37.90(36.84–38.97) | III+MS |
| I319 | 0.04(0.03–0.05) | 0.84(0.81–0.86) | 2.12(2.00–2.24) | 0.33(0.31–0.35) | 11.27(10.68–11.87) | 26.54(25.68–27.41) | III+MS |
| I324 | 0.12(0.12–0.13) | 1.01(0.99–1.04) | 3.28(3.11–3.45) | 0.20(0.19–0.21) | 46.24(44.97–47.49) | 69.48(67.68–71.25) | III+MS |
| I326 | 0.07(0.06–0.09) | 0.81(0.77–0.85) | 2.75(2.27–3.40) | 0.29(0.26–0.31) | 5.53(5.14–5.91) | 7.12(6.55–7.68) | III+MS |
| I328 | 0.11(0.11–0.12) | 0.65(0.62–0.68) | 1.36(1.33–1.40) | 0.19(0.18–0.20) | 18.43(17.43–19.45) | 50.93(49.76–52.11) | III+MS |
| I343 | 0.19(0.18–0.19) | 0.68(0.66–0.70) | 1.77(1.73–1.81) | 0.31(0.30–0.32) | 29.90(28.63–31.18) | 75.64(74.08–77.22) | other |
| I346 | 0.06(0.05–0.07) | 0.78(0.75–0.81) | 1.97(1.81–2.15) | 0.49(0.47–0.52) | 10.17(9.65–10.69) | 13.13(12.45–13.81) | II |
| S2 | 0.00(0.00–0.01) | 0.64(0.60–0.68) | 1.64(1.57–1.72) | 0.73(0.70–0.76) | 7.42(6.97–7.86) | 14.14(13.52–14.76) | III+MS |

[a]Accepted fits are listed.

[b]The lower and upper boundary for 1 $\sigma$ confidence level are given in parentheses.

[c]Best-fit value of the lower temperature component.

[d]Best-fit value of the higher temperature component.

[e]The absorption and the metallicity of the higher temperature component is fixed to be the same with those of the lower temperature component. The best fit value of temperature and metallicity are searched for in the range of less than 20 keV and 5 solar respectively.

[f]Luminosity of each component in 0.5–8.0 keV band (corrected for absorption)

[g]Abundance relative to solar photospheric (Morrison & McCammon 1983).

[h]Classification based on the $J$, $H$, and $K_s$-band magnitude of 2MASS counterpart. "I" for class I, "II" for class II, and "III+MS" for class III+MS. "others" are for sources which are out of these groups. " $\cdots$ " sources can not be classified due to their lack of a NIR counterpart.

TABLE 4

X-RAY PROPERTIES OF EACH CLASS

| | Class I | Class II | Class III+MS |
|---|---|---|---|
| Frequency ..... | 19 | 18 | 61 |
| Sources with time-variation . | 6 (32%) | 10 (56%) | 21 (34%) |
| Source with two temperature | 1 ( 5%) | 3 (17%) | 15 (25%) |
| Absorption($10^{22}$cm$^{-2}$)[a]..... | 2.49(2.37–2.62) | 0.63(0.60–0.67) | 0.11(0.10–0.13) |
| Metallicity (solar)[ab]..... | 0.82(0.61–0.99) | 0.60(0.50–0.69) | 0.20(0.18–0.22) |
| Temperature (keV)[a]..... | 2.99(2.66–3.57) | 2.91(2.63–3.26) | 1.20(1.13–1.28) |
| Luminosity ($10^{29}$erg s$^{-1}$)[a]... | 49.1(46.7–51.5) | 36.3(35.1–37.5) | 36.4(35.7–37.0) |

[a]The lower and upper boundary for 1 $\sigma$ confidence level are given in parentheses.

[b]Abundance relative to solar photospheric (Morrison & McCammon 1983).